Stability and time-step constraints of implicit-explicit Runge–Kutta methods for the linearized Korteweg–de Vries equation

Joseph Hunter* Zheng Sun† Yulong Xing‡

Abstract

This paper provides a study on the stability and time-step constraints of solving the linearized Korteweg–de Vries (KdV) equation, using implicit-explicit (IMEX) Runge-Kutta (RK) time integration methods combined with either finite difference or local discontinuous Galerkin spatial discretization. We analyze the stability of the fully discrete scheme, on a uniform mesh with periodic boundary conditions, using the Fourier method. For the linearized KdV equation, the IMEX schemes are stable under the standard CFL condition $\tau \leq \hat{\lambda} h$. Here $\hat{\lambda}$ is the CFL number, τ is the time-step size, and h is the spatial mesh size. We study several IMEX schemes and characterize their CFL number as a function of $\theta = d/h^2$ with d being the dispersion coefficient, which leads to several interesting observations. We also investigate the asymptotic behaviors of the CFL number for sufficiently refined meshes and derive the necessary conditions for the asymptotic stability of the IMEX-RK methods. Some numerical experiments are provided in the paper to illustrate the performance of IMEX methods under different time-step constraints.

Keywords: linearized Korteweg-de Vries equation, implicit-explicit Runge–Kutta method, stability, CFL condition, finite difference method, local discontinuous Galerkin method

2020 Mathematics Subject Classifications: 65M12, 65M60, 65M06

1 Introduction

In this paper, we study the stability and time-step constraints for solving the following linearized Korteweg–de Vries (KdV) equation, also regarded as the linear convection-dispersion equation, using implicit-explicit (IMEX) Runge–Kutta (RK) time integration methods:

$$u_t + u_x + d u_{xxx} = 0, \quad u = u(x,t), \quad (x,t) \in (0, 2\pi) \times (0, T), \tag{1.1}$$

where $d > 0$ is a constant associated with the strength of the dispersion. For spatial discretization, a finite difference (FD) or a discontinuous Galerkin (DG) finite element method can be used. We will analyze the stability of the fully discrete scheme via the Fourier method, therefore, the analysis of the paper is built upon the essential assumptions that the problem is linear and is solved on a uniform mesh with periodic boundary conditions. We focus on this simple setup and hope it will provide insight into the numerical performance of the IMEX schemes when applied to nonlinear dispersive wave equations under a more general setting.

In the use of an IMEX time integration method, one usually treats the linear stiff term implicitly while handling the non-stiff nonlinear term explicitly. In this way, the IMEX method can allow a much larger time-step size compared with a purely explicit method and avoid inversion of nonlinear systems compared with a purely implicit method. Due to these advantages, IMEX methods are widely used for the numerical discretization of different types of equations, such as the convection-reaction/diffusion/dispersion equations, hyperbolic systems with relaxation terms, and kinetic equations. Over the past three decades, both IMEX-RK and IMEX multistep methods have been developed to accomplish these tasks, and we refer to [4, 3, 1, 2, 8, 24, 21, 7, 17] for an incomplete list of references.

*Department of Mathematics, The Ohio State University, Columbus, OH 43210, USA. E-mail: hunter.926@osu.edu.
†Department of Mathematics, The University of Alabama, Tuscaloosa, AL 35487, USA. E-mail: zsun30@ua.edu.
‡Department of Mathematics, The Ohio State University, Columbus, OH 43210, USA. E-mail: xing.205@osu.edu.

For mathematical models containing higher-order spatial derivatives, utilizing IMEX time-marching methods by treating the higher-order derivative terms implicitly may improve the stability condition. For the convection-diffusion equation, the time-step constraint can be improved from $\tau \le Ch^2$ (for explicit time stepping) to $\tau \le \max(Ch, \tau_0)$ (for IMEX time stepping) [31], where τ, h are the time-step and spatial mesh sizes, respectively, and τ_0 is a constant. For the third-order linear convection-dispersion equation, a purely explicit method typically requires a restrictive time-step constraint $\tau \le Ch^3$ for stability. There have been some studies on the stability condition when an IMEX time-marching method is used. In [15], the stability of several IMEX methods coupled with finite volume spatial discretization for the nonlinear KdV equation is studied numerically, and it was observed that such method is stable under the standard Courant–Friedrichs–Lewy (CFL) condition $\tau \le \hat{\lambda} h$. Here the constant $\hat{\lambda}$ is referred to as the CFL number. When an FD spatial discretization is considered, Fourier analysis was carried out in [28] for the linear convection-dispersion equation to validate such CFL conditions. In [28], it is pointed out that the CFL number $\hat{\lambda}$ may vary with the dispersion constant d, and for the three IMEX schemes studied in [28], the CFL condition for the pure convection case ($d = 0$) also seems to be a sufficient stability condition for the general case $d > 0$.

In this paper, we aim to further investigate the stability and time-step constraints of IMEX schemes for solving the linearized KdV equation (1.1). We focus on IMEX-RK time marching and consider both the FD method and the local DG method for spatial discretization. The local DG method was first introduced by Cockburn and Shu in [11] for the convection-diffusion equation, motivated by the successful numerical experiments by Bassi and Rebay in [5]. Then it was extended to KdV-type equations in [33] and many other time-dependent problems with high-order spatial derivatives. See [32, 6, 14, 13, 30, 22, 27, 23, 25] and references therein for an incomplete list. In this paper, we will apply the spatial discretization in [33, 20] and refer to it as the DG scheme for simplicity. The main theoretical tool used in the paper is the von Neumann type analysis based on analyzing the scheme with Fourier ansatz. Such analysis is standard for finite difference methods. For DG methods, such analysis has also been frequently used in [35, 36, 18, 34, 9, 10, 16, 29].

In the first part of the paper, we aim at better characterizing the CFL number $\hat{\lambda}$ when solving (1.1) with an IMEX scheme. We have applied the von Neumann type analysis to several IMEX methods coupled with FD or DG spatial discretization to study their stability requirements. The $\hat{\lambda}-\theta$ curves for four specific IMEX-RK methods are provided. We also examined the sharpness of such CFL conditions by solving (1.1) with an initial sine wave numerically. Some interesting observations are summarized as follows.

- The maximum CFL number $\hat{\lambda} = \hat{\lambda}(\theta)$ based on the von Neumann type analysis is a function of $\theta := d/h^2$, where d is the dispersion constant in (1.1) and h is the spatial mesh size. As a result, in terms of stability, solving (1.1) on a coarse mesh is similar to solving a convection-dominated problem (i.e., for fixed θ, a large h corresponds to a small d), and solving (1.1) on a fine mesh is similar to solving a dispersion-dominated problem (i.e., for fixed θ, a small h corresponds to a large d).

- In general, $\hat{\lambda}(\theta)$ is not a non-decreasing function of θ. In other words, it is possible that $\hat{\lambda}(0) > \hat{\lambda}(\theta)$, i.e., the CFL condition of the IMEX scheme for $d > 0$ could possibly be more restrictive than the CFL condition for the corresponding explicit scheme for the pure convection equation ($d = 0$).

- Since the CFL number may vary in different regimes of θ (or equivalently, h), in a numerical test that we fix the ratio τ/h, it is possible that the numerical solution "blows up" on a coarse mesh, but then converges to the exact solution after mesh refinement.

In the second part of the paper, as an effort of understanding the stability of numerical schemes on sufficiently refined meshes ($h \to 0$ and $\theta = d/h^2 \to \infty$), we investigate the asymptotic behaviors of $\hat{\lambda}(\theta)$ as $\theta \to \infty$. In particular, we want to know what condition we should impose on coefficients in the Butcher tableaux of IMEX methods to ensure that $\hat{\lambda}_\infty := \lim_{\theta\to\infty} \hat{\lambda}(\theta) > 0$ in the limit $\theta \to \infty$. Unfortunately, at this moment, we are not able to derive a sufficient condition. Instead, only necessary conditions are acquired for the asymptotic stability of the IMEX-RK methods, which may help us rule out some "bad" schemes. This necessary condition roughly requires that the stability function $\phi(\cdot)$ of the implicit scheme in the IMEX-RK scheme satisfies $|\phi(-\infty)| := |\lim_{\zeta\to-\infty} \phi(\zeta)| < 1$. We have also

constructed several second-order two-stage IMEX methods as a simple test case to provide further examinations and shed more information on whether the necessary condition is also sufficient.

The rest of the paper is organized as follows. In Section 2, we briefly outline the background and preliminaries of this paper. In Section 3, we study the CFL conditions by analyzing the spectral radius of the amplification matrices of the schemes. Four IMEX-RK methods are studied in detail. Some numerical experiments are also provided. In Section 4, we derive a necessary condition for the CFL number to be positive in the asymptotics $\theta \to \infty$. Finally, conclusions are given in Section 5.

2 Background and preliminaries

In this section, we will briefly review the FD and local DG spatial discretization for (1.1), the IMEX time discretization, and Fourier analysis of the numerical scheme.

2.1 FD spatial discretization

Consider a uniform grid $\{x_j\}_{j=0}^{N-1}$ over $[0, 2\pi)$ with N points. The mesh size is $h = 2\pi/N$ and $x_j = jh$. The numerical solution over the grid is represented as $\{u_j\}_{j=0}^{N-1}$. Instead of considering a specific FD discretization, we consider a general FD discretization of the form $u_x \approx \mathcal{C}(u)$ and $u_{xxx} \approx \mathcal{D}(u)$, for some FD operators $\mathcal{C}(\cdot)$ and $\mathcal{D}(\cdot)$. The semidiscrete scheme is then given by

$$u' = -\mathcal{C}(u) - d\mathcal{D}(u). \tag{2.1}$$

As an example, the following FD discretization used in [28]

$$u_x\big|_{x=x_j} \approx \mathcal{C}(u)\big|_j := \frac{3u_j + 2u_{j+1} - 6u_{j-1} + u_{j-2}}{6h},$$

and

$$u_{xxx}\big|_{x=x_j} \approx \mathcal{D}(u)\big|_j := \frac{-u_{j+3} + 7u_{j+2} - 14u_{j+1} + 10u_j - u_{j-1} - u_{j-2}}{4h^3},$$

will be studied in Section 3. This FD scheme has third-order accuracy. In Section 4, we will consider a generic FD scheme without specifying the operators $\mathcal{C}(\cdot)$ and $\mathcal{D}(\cdot)$.

2.2 Local DG spatial discretization

In the DG method, the computational domain is partitioned into N cells. We assume uniform meshes to facilitate the Fourier analysis in the later section. The cells are denoted as $I_j = (x_{j-1/2}, x_{j+1/2})$ for $1 \le j \le N$. The length of the cell will be denoted as $h = x_{j+1/2} - x_{j-1/2}$. The numerical solution is defined on the finite element space V_h^k consisting of piecewise polynomials

$$V_h^k = \{v : v|_{I_j} \in P^k(I_j), 1 \le j \le N\},$$

where $P^k(I_j)$ is the linear space on I_j spanned by polynomials of degree less than or equal to k. We will refer to this construction as a P^k-DG method. The method does not rely on a specific polynomial basis, but when necessary, we will take the following basis of V_h^k for our analysis

$$V_h^k = \text{span}\{\psi_{j,0}, ..., \psi_{j,k} : 1 \le j \le N\},$$

where $\psi_{j,k}$ is the normalized kth-order Legendre polynomial on the cell I_j and is zero on all other cells.

Applying the local DG method [33] to (1.1) results in the semi-discrete form which is defined as follows: Find $u, p, q \in V_h^k$ such that for all test functions $v, w, z \in V_h^k$ we have

$$\int_{I_j} u_t v \,\mathrm{d}x - \int_{I_j} (u+p)v_x \,\mathrm{d}x + (\hat{u}+\hat{p})_{j+1/2} v^-_{j+1/2} - (\hat{u}+\hat{p})_{j-1/2} v^+_{j-1/2} = 0, \tag{2.2a}$$

$$\int_{I_j} pw \,\mathrm{d}x + \int_{I_j} qw_x \,\mathrm{d}x - \hat{q}_{j+1/2} w^-_{j+1/2} + \hat{q}_{j-1/2} w^+_{j-1/2} = 0, \tag{2.2b}$$

$$\int_{I_j} qz \,\mathrm{d}x + d\left(\int_{I_j} uz_x \,\mathrm{d}x - \hat{u}_{j+1/2} z^-_{j+1/2} + \hat{u}_{j-1/2} z^+_{j-1/2} \right) = 0. \tag{2.2c}$$

Hat terms are numerical fluxes which are defined as

$$\hat{u} = u^-, \qquad \hat{q} = q^+, \qquad \hat{p} = p^+$$

in this paper. Here $v^-_{j+1/2}$ denotes the left limit of v at $x_{j+1/2}$ from I_j; and $v^+_{j+1/2}$ is defined similarly as the right limit at $x_{j+1/2}$ from I_{j+1}.

By specifying a set of basis functions, (2.2) can be written in a similar form as an FD scheme. First, we note that the solutions u, p, and q are elements of V_h^k, and they can be written as linear combinations of $\psi_{j,k}$. For example, on the cell I_j,

$$u(x) = u_{j,0}\psi_{j,0} + u_{j,1}\psi_{j,1} + ... + u_{j,k}\psi_{j,k}.$$

Then by taking the test function as $\psi_{j,0}, \psi_{j,1}, ..., \psi_{j,k}$ respectively, each equation in (2.2) becomes a system of $(k+1)$ equations with respect to the basis coefficients. After substituting the resulted systems of (2.2b) and (2.2c) into that of (2.2a), one can get a simplified system of the form

$$u_j' = \frac{1}{h}\left(C_1 u_j + C_2 u_{j-1}\right) + \frac{d}{h^3}\left(D_1 u_{j+2} + D_2 u_{j+1} + D_3 u_j + D_4 u_{j-1}\right), \tag{2.3}$$

where $u_j = [u_{j,0}, u_{j,1}, ..., u_{j,k}]^T$; C_1 and C_2 are $(k+1)\times(k+1)$ coefficient matrices which arise from the discretization of u_x; and D_1, D_2, D_3, and D_4 are $(k+1)\times(k+1)$ coefficient matrices which arise from the discretization of u_{xxx}.

2.3 IMEX time discretization

For time discretization we will use IMEX-RK methods. An IMEX method can be represented by the following Butcher tableaux:

$$\begin{array}{c|c} c & A \\ \hline & b^T \end{array} \qquad\qquad \begin{array}{c|c} \tilde{c} & \tilde{A} \\ \hline & \tilde{b}^T \end{array}$$

where $A = [a_{ij}]$ and $\tilde{A} = [\tilde{a}_{ij}]$ with $\tilde{a}_{ij} = 0$ for $j \geq i$ are $s \times s$ matrices; $\tilde{c} = [\tilde{c}_1, \cdots, \tilde{c}_s]^T$, $c = [c_1, \cdots, c_s]^T$, $\tilde{b} = [\tilde{b}_1, \cdots, \tilde{b}_s]$, and $b = [b_1, \cdots, b_s]$ are s-vectors. The tableau on the left is for the implicit method, and the tableau on the right is for the explicit method. The implicit method will be applied to the part of the equation arising from u_{xxx}, and the explicit method will be applied to the part of the equation arising from u_x. We will say an IMEX method is A-stable if the implicit method is A-stable, and an L-stable IMEX method is defined in the same fashion. Moreover, we will focus on diagonally implicit methods, meaning $a_{ij} = 0$ for $j > i$. These methods are easier to implement and are favored in many applications. Applying a diagonally implicit IMEX-RK method to an equation of the form

$$\hat{u}' = \frac{1}{h} C\hat{u} + \frac{d}{h^3} D\hat{u} \tag{2.4}$$

results in the following sets of equations

$$\begin{aligned} \hat{u}^{n,i} =& \hat{u}^n + \frac{\tau}{h}\sum_{j=1}^{i-1} \tilde{a}_{i,j} C\hat{u}^{n,j} + \frac{d}{h^2}\frac{\tau}{h}\sum_{j=1}^{i} a_{i,j} D\hat{u}^{n,j} \qquad \text{for } 1 \leq i \leq s, \\ \hat{u}^{n+1} =& \hat{u}^n + \frac{\tau}{h}\sum_{j=1}^{s} \tilde{b}_j C\hat{u}^{n,j} + \frac{d}{h^2}\frac{\tau}{h}\sum_{j=1}^{s} b_j D\hat{u}^{n,j}. \end{aligned}$$

Here $\tau = t^{n+1} - t^n$ is the size of the time step.

In the latter sections, we will use the triplet (s, σ, p) to denote an s-stage implicit, σ-stage explicit, order p IMEX method. In particular, the following IMEX methods will be investigated in detail in Section 3. The methods described by (2.5) and (2.7) come from [3], the method (2.6) comes from [24], the method (2.8) comes from [3] (also in [15], referred to as "with larger dissipative region"), and the method (2.9) comes from [8] (see also [31, 28]).

L-stable second-order DIRK (2,2,2) [3]

$$\begin{array}{c|ccc|ccc} 0 & 0 & 0 & 0 & 0 & 0 & 0 \\ \gamma & 0 & \gamma & 0 & \gamma & 0 & 0 \\ 1 & 0 & 1-\gamma & \gamma & \delta & 1-\delta & 0 \\ \hline & 0 & 1-\gamma & \gamma & \delta & 1-\delta & 0 \end{array} \tag{2.5}$$

$$\gamma = 1 - \frac{\sqrt{2}}{2} \text{ and } \delta = 1 - \frac{1}{2\gamma}$$

Third-order IMEXSSP3 (4,3,3) [24]

$$\begin{array}{c|cccc} \alpha & \alpha & 0 & 0 & 0 \\ 0 & -\alpha & \alpha & 0 & 0 \\ 1 & 0 & 1-\alpha & \alpha & 0 \\ 1/2 & \beta & \eta & 1/2-\beta-\eta-\alpha & \alpha \\ \hline & 0 & 1/6 & 1/6 & 2/3 \end{array} \qquad \begin{array}{c|cccc} 0 & 0 & 0 & 0 & 0 \\ 0 & 0 & 0 & 0 & 0 \\ 1 & 0 & 1 & 0 & 0 \\ 1/2 & 0 & 1/4 & 1/4 & 0 \\ \hline & 0 & 1/6 & 1/6 & 2/3 \end{array} \tag{2.6}$$

$$\alpha = 0.24219426078821,\ \beta = 0.06042356519705, \text{ and } \eta = 0.12915286960590$$

Third-order combination (2,3,3) [3]

$$\begin{array}{c|ccc|ccc} 0 & 0 & 0 & 0 & 0 & 0 & 0 \\ \gamma & 0 & \gamma & 0 & \gamma & 0 & 0 \\ 1-\gamma & 0 & 1-2\gamma & \gamma & \gamma-1 & 2(1-\gamma) & 0 \\ \hline & 0 & 1/2 & 1/2 & 0 & 1/2 & 1/2 \end{array} \tag{2.7}$$

$$\gamma = \tfrac{3+\sqrt{3}}{6}$$

L-stable third-order DIRK (3,4,3) [3]

$$\begin{array}{c|cccc|cccc} 0 & 0 & 0 & 0 & 0 & 0 & 0 & 0 & 0 \\ \gamma & 0 & \gamma & 0 & 0 & \gamma & 0 & 0 & 0 \\ \frac{1+\gamma}{2} & 0 & \frac{1-\gamma}{2} & \gamma & 0 & a_{31} & a_{32} & 0 & 0 \\ 1 & 0 & b_1 & b_2 & \gamma & a_{41} & a_{42} & a_{43} & 0 \\ \hline & 0 & b_1 & b_2 & \gamma & 0 & b_1 & b_2 & \gamma \end{array} \tag{2.8}$$

$$\gamma = 0.4358665215,\ a_{31} = 0.3212788860,\ a_{32} = 0.3966543747,\ a_{41} = -0.105858296,$$
$$a_{42} = a_{43} = 0.5529291479,\ b_1 = 1.208496649,\ b_2 = -0.644363171$$

Alternate L-stable third-order DIRK (3,4,3) [8]

$$\begin{array}{c|cccc|cccc} 0 & 0 & 0 & 0 & 0 & 0 & 0 & 0 & 0 \\ \gamma & 0 & \gamma & 0 & 0 & \gamma & 0 & 0 & 0 \\ \frac{1+\gamma}{2} & 0 & \frac{1-\gamma}{2} & \gamma & 0 & \frac{1+\gamma}{2}-a_1 & a_1 & 0 & 0 \\ 1 & 0 & b_1 & b_2 & \gamma & 0 & 1-a_2 & a_2 & 0 \\ \hline & 0 & b_1 & b_2 & \gamma & 0 & b_1 & b_2 & \gamma \end{array} \tag{2.9}$$

$$\gamma = 0.4358665215,\ a_1 = -0.35,\ a_2 = \frac{1/3 - 2\gamma^2 - 2b_2a_1\gamma}{\gamma(1-\gamma)},\ b_1 = 1.208496649,\ b_2 = -0.644363171$$

2.4 Fourier analysis

To analyze the time-step constraint of the IMEX methods when paired with an FD or a DG space discretization, the Fourier method is used. The ansatz of the form

$$u_j = \hat{u}e^{i\omega x_j}, \quad \text{with } i \text{ being the imaginary unit,}$$

is substituted into the numerical schemes. For the DG method, the substitution into (2.3) yields the ordinary differential equations in the form of (2.4), where $C = C_1 + C_2e^{-iz}$ and $D = D_1e^{2iz} + D_2e^{iz} +$

$D_3 + D_4 e^{-iz}$ with $z = \omega h$. A similar equation can be derived for an FD scheme by making the same ansatz substitution into equation (2.1).

The IMEX method of interest is then applied to equation (2.4), and the value of $\hat{u}$ at the time-step t^{n+1} satisfies

$$\hat{u}^{n+1} = K(z, \lambda, \theta)\hat{u}^n. \tag{2.10}$$

Here we have

$$z = \omega h, \quad \lambda = \frac{\tau}{h}, \quad \text{and} \quad \theta = \frac{d}{h^2}.$$

The choice of $\theta = d/h^2$ will be made clear in the next section. Note K is a polynomial of matrices C and D, which are 2π-periodic in z. Hence we only need to consider $z \in [0, 2\pi)$ in (2.10). If an FD discretization is used, K is a scalar, which depends on the parameters z, λ, and θ. If a P^k-DG method is used, K is a $(k+1) \times (k+1)$ matrix, which depends on the above parameters. In particular, when $z = 0$ or $\lambda = 0$, we have $K = 1$ in an FD method, and $K = I$ is the identity matrix in a DG method, meaning that the numerical scheme will not evolve a constant solution or as the time-step size is zero.

The following condition asserts when the fully discrete scheme will be (strongly) stable.

Theorem 2.1. *Given $\lambda = \tau/h$ and $\theta = d/h^2$,*

1. *for an FD method, if $|K(z, \lambda, \theta)| \le 1$ for all z, then the method is stable;*
2. *for a DG method, if K is uniformly diagonalizable and $\rho(K(z, \lambda, \theta)) \le 1$ for all z, then the method is stable. Here $\rho(K)$ is the spectral radius of K.*

Remark 2.2. *Theorem 2.1 guarantees the strong stability of the numerical scheme, namely $|\hat{u}^{n+1}| \le |\hat{u}^n|$ is monotonously nonincreasing. In practice, to ensure that the numerical scheme works appropriately, a weaker stability condition can be imposed, namely, $|K(z, \lambda, \theta)| \le 1 + \mu\tau$ for some fixed constant μ. However, this condition is much more difficult to be verified. We hence require $|K| \le 1$ in our latter sections, where $|K|$ refers to either the absolute value of the scalar K or the spectral radius of the matrix K.*

3 Studies of CFL conditions for specific IMEX schemes

Our aim is to investigate whether the IMEX-FD and IMEX-DG methods are stable under certain CFL-type conditions $\lambda = \tau/h \le \hat{\lambda}$. Motivated by Theorem 2.1, for a given value of θ, we define the maximum allowable λ as

$$\hat{\lambda} = \hat{\lambda}(\theta) = \sup\left\{\tilde{\lambda} : \rho\left(K\left(z, \lambda, \theta\right)\right) \le 1, \forall\, 0 \le z < 2\pi,\, 0 \le \lambda \le \tilde{\lambda}\right\}, \tag{3.1}$$

From a practical standpoint, we will focus on and investigate the following values of $\hat{\lambda}$.

- $\hat{\lambda}_{\min} := \inf_{\theta > 0} \hat{\lambda}(\theta)$, the global minimum value of $\hat{\lambda}$. This corresponds to the time-step constraint for all regimes of d and for all mesh sizes h.
- $\hat{\lambda}_{\infty} := \lim_{\theta \to \infty} \hat{\lambda}(\theta)$, the value of $\hat{\lambda}$ as $\theta = d/h^2 \to \infty$. This gives the time-step constraint as the spatial mesh is sufficiently refined ($h \to 0$).

Remark 3.1. *For $d = 0$, the PDE (1.1) reduces to*

$$u_t + u_x = 0.$$

The corresponding CFL condition has already been studied in [12, Table 2.2] numerically for pth-order RK methods with p stages. This corresponds to the value of $\hat{\lambda}(0)$.

3.1 Numerical approach for finding $\hat{\lambda}(\theta)$

Given an IMEX-FD or an IMEX-DG method, we numerically compute the time-step size $\hat{\lambda}(\theta)$ with various different values of θ. For each fixed θ, we sampled z densely with 10001 evenly spaced points over the interval $[0, 2\pi]$. Then we start with $\tilde{\lambda} = 0$ and examined whether $\rho(K(z, \tilde{\lambda}, \theta)) \leq 1 + \varepsilon$ for all sampled z, where $\varepsilon = 10^{-16}$ is used as a relaxation term. If yes, we increased the value of $\tilde{\lambda}$. Otherwise, we recorded the previous value of $\tilde{\lambda}$ as an estimate of $\hat{\lambda}(\theta)$.

Before proceeding further, we verify that $\hat{\lambda}$ is indeed a function of $\theta = d/h^2$. In other words, for any $d_1, h_1, d_2, h_2 > 0$, if $d_1/h_1^2 = \theta = d_2/h_2^2$, then $\hat{\lambda}(d_1/h_1^2) = \hat{\lambda}(d_2/h_2^2)$. This claim is examined in Figure 1 for the $(2, 2, 2)$ L-stable method (2.5), where we computed the value of $\hat{\lambda}$ for $h = 1, 0.1, 0.01, 0.001$ with a varying d. It can be seen that the graph preserves the same pattern and shifts points left by two powers of 10 as h is decreased by a power of 10. We have also tested this for other IMEX methods and examined different values of h. Similar numerical results are observed.

Note that $\theta \to \infty$ when $h \to 0$. Therefore, as pointed out previously, $\hat{\lambda}_\infty$ corresponds to the CFL condition as the mesh is sufficiently refined.

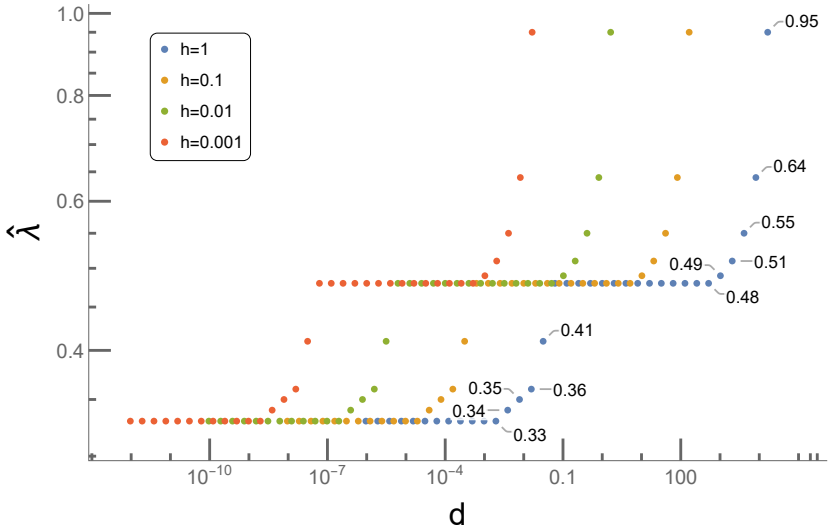

Figure 1: Comparison of $\hat{\lambda}$ for the second-order L-stable method using P^k-DG with $k = 1$, where d varies and h is fixed.

3.2 Main results from spectral analysis

We tested four IMEX methods (2.5)-(2.8), which include a second-order method and three third-order methods, to study their CFL condition using the spectral analysis in Section 2.4. For spatial discretizations, we will consider both the FD method in Section 2.1 and the DG method in Section 2.2. The second-order IMEX method is coupled with a P^1-DG method and the third-order IMEX methods are coupled with a P^2-DG method.

Then we present the discrete plot of $\hat{\lambda}(\theta)$ with different spatial discretizations in Figure 2. The corresponding limit values $\hat{\lambda}_\infty$ and infimum values $\hat{\lambda}_{\min}$ are recorded in Table 1. Based on these results, we have the following observations:

1. ($\hat{\lambda}(\theta)$ may not be non-decreasing.) In general, $\hat{\lambda}(\theta)$ is not a non-decreasing function of θ. In other words, as θ increases, or as the dispersive term starts to dominate, although the implicit solver plays a more important role in the full IMEX discretization, the time-step constraint could possibly become worse. This indicates that the implicit scheme in the IMEX method does not always help stabilize the scheme.

   However, certain IMEX methods seem to suffer less from this fact. For example, for the second and third-order L-stable methods, we do typically get a more relaxed CFL condition as θ grows.

2. (Regime of large θ.) $\hat{\lambda}_\infty$ may exhibit different asymptotic behaviors in different schemes, either growing to infinity or tending to a fixed constant. We remark that in the later case, it is possible that $\hat{\lambda}_\infty$ shrinks to zero, as will be seen in Figure 4d with the P^1-DG method. We have also observed a similar behavior, $\hat{\lambda}_\infty \approx 0$, when the third-order FD method is used, and the plot is omitted.

3. (Different spatial discretizations.) In general, it seems that the FD schemes have a more relaxed CFL condition compared with the DG schemes. For some IMEX methods, we observe that the $\hat{\lambda}-\theta$ curves may share similar patterns despite the use of the FD or the DG spatial discretizations. But the pattern may not be quite clear for some other methods, such as the IMEXSSP3 method.

4. (The "best" third-order method.) Among the three third-order methods and for both the FD and DG spatial discretizations, the third-order L-stable method attains the largest value of $\hat{\lambda}_{\min}$, meaning that it has the best overall performance in all regimes; while the IMEXSSP3 method attains the largest value of $\hat{\lambda}_\infty$, meaning that the IMEXSSP3 method works the best for the dispersion-dominated case or on very refined meshes. We have also tested the coupling of the third-order L-stable method with the P^3-DG methods, which gives $\hat{\lambda}_\infty = 0.49$ and $\hat{\lambda}_{\min} = 0.14$. The IMEXSSP3 method coupled with P^3-DG gives $\hat{\lambda}_\infty = \infty$ and $\hat{\lambda}_{\min} = 0.0001$.

order p	method	$\hat{\lambda}_\infty$		$\hat{\lambda}_{\min}$	
		FD	P^{p-1}-DG	FD	P^{p-1}-DG
2	L-stable	∞	∞	0.87	0.33
3	IMEXSSP3	8	∞	1.67	0.002
3	Combination	0.87	0.17	0.87	0.17
3	L-stable	6.29	0.79	1.74	0.23

Table 1: $\hat{\lambda}_\infty$ and $\hat{\lambda}_{\min}$ for four methods studied.

3.3 Numerical experiments

In this subsection, we will use the following problem [28] to examine the time-step constraints in the actual computation:

$$\begin{cases} u_t + u_x + du_{xxx} = 0, & (x,t) \in (0,2\pi) \times (0,T), \\ u(x,0) = \sin(x), & x \in (0,2\pi). \end{cases} \tag{3.2}$$

The periodic boundary condition is imposed, and its exact solution is given by $u(x,t) = \sin(x-(1-d)t)$.

In each of our numerical tests, we fix the value of $d > 0$ and the CFL number λ, and observe whether the numerical solutions would blow up as we refine the mesh. Note as the mesh size h decreases, the ratio $\theta = d/h^2$ increases. This will cause some complications in the numerical experiments as we will explain in further detail later.

3.3.1 Examples that $\rho(K) \le 1$ gives a sharp CFL condition

First, we aim to demonstrate that the $\hat{\lambda}$ values obtained by verifying $\rho(K) \le 1$, although being a stronger stability condition as studied in Theorem 2.1, can provide sharp bounds at least for some of the numerical schemes.

For example, for the third-order combination method, in the tail region where $\hat{\lambda}(\theta) \approx 0.18$. A slightly larger value of λ will cause the blowup of numerical solutions, which can be observed from the numerical error reported in Table 2. Table 3 shows similar results for the third-order L-stable method and its tail region with $\hat{\lambda}(\theta) \approx 0.797$.

3.3.2 Examples that $\rho(K) \le 1$ does not give a sharp CFL condition

Next, we remark that in some cases, the numerical methods may remain "stable" under a time-step constraint $\tau = \lambda h$ with $\lambda > \hat{\lambda}(\theta)$. In this case, the strong stability condition $\rho\left(K(z,\lambda,\theta)\right) \le 1$ no

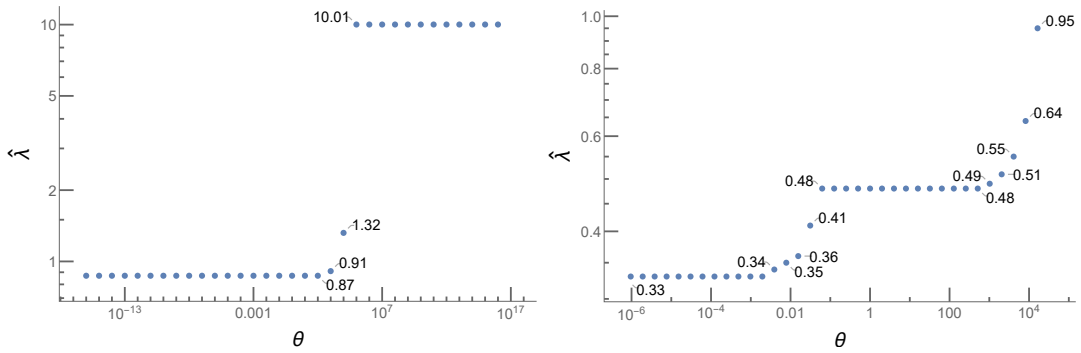

(a) second-order L-stable, third-order FD ($\hat{\lambda}$ capped at 10)

(b) second-order L-stable, P^1-DG

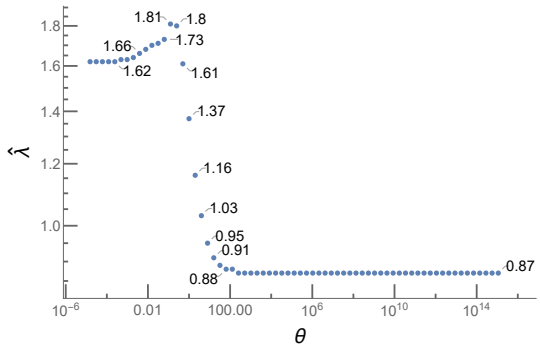

(c) third-order combination, third-order FD

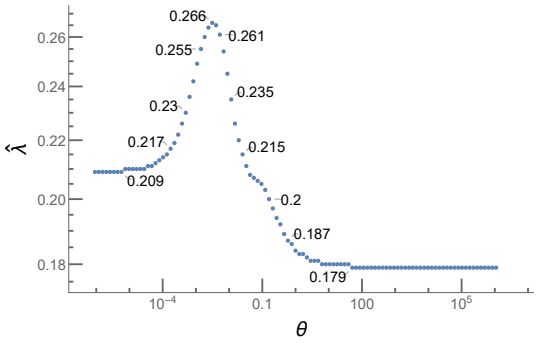

(d) third-order combination, P^2-DG

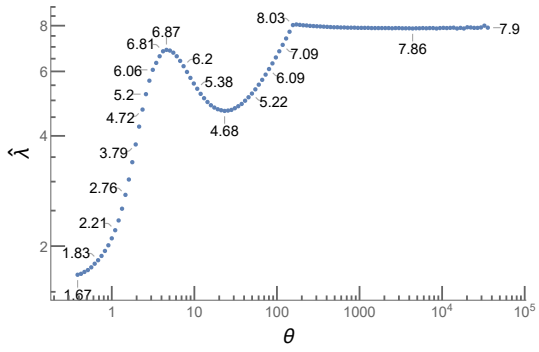

(e) IMEXSSP3, third-order FD

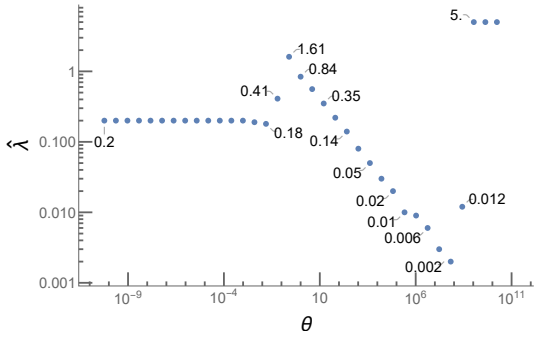

(f) IMEXSSP3, P^2-DG ($\hat{\lambda}$ capped at 5)

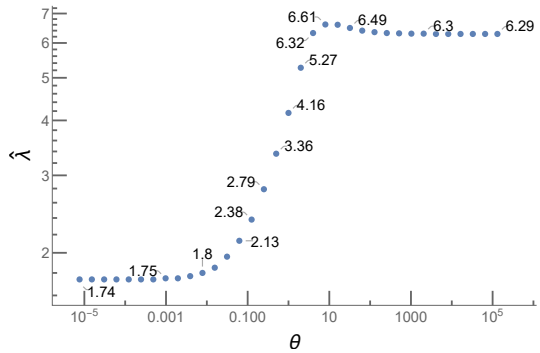

(g) third-order L-stable, third-order FD

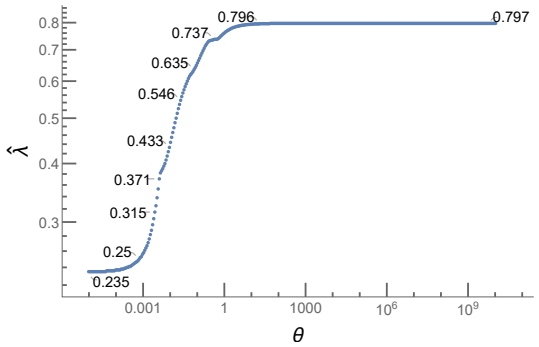

(h) third-order L-stable, P^2-DG

Figure 2: $\hat{\lambda} - \theta$ curves of different IMEX methods with the third-order FD and the P^k-DG spatial discretizations.

λ	N	θ	L^2 error	order
0.18	10	1.2665	4.3239e-02	–
	20	5.0661	4.4106e-03	3.29
	40	20.264	5.1829e-04	3.09
	80	81.057	6.3694e-05	3.02
	160	324.23	7.9061e-06	3.01
0.19	10	1.2665	1.4193e+08	–
	20	5.0661	1.1443e+27	-62.81
	40	20.264	5.4828e+58	-105.24
	80	81.057	3.8008e+122	-212.07
	160	324.23	4.0283e+258	-451.87

Table 2: Third-order combination method coupled with a P^2-DG method. Comparison between $\lambda = 0.18$ and $\lambda = 0.19$ with $d = 0.5$ at $T = 100$.

λ	N	θ	L^2 error	order
0.79	10	1.2665	5.0304e-01	–
	20	5.0661	6.1198e-02	3.04
	40	20.264	7.5404e-03	3.02
	80	81.057	9.3861e-04	3.01
	160	324.23	1.1727e-04	3.00
0.81	10	1.2665	5.4117e-01	–
	20	5.0661	6.5966e-02	3.04
	40	20.264	8.1275e-03	3.02
	80	81.057	1.1614e-00	-7.16
	160	324.23	3.8355e+10	-34.9
0.83	10	1.2665	5.8333e-01	–
	20	5.0661	7.0900e-02	3.04
	40	20.264	3.2829e+02	-12.18
	80	81.057	1.0843e+16	-44.91
	160	324.23	6.0073e+42	-88.84

Table 3: Third-order L-stable method coupled with a P^2-DG method. Comparison of $\lambda = 0.79, 0.81, 0.83$ with $d = 0.5$ and $T = 100$.

longer holds, and the norm of the numerical solution may grow, which means that the method may be working under the "weak" stability.

For example, consider the L-stable $(3, 4, 3)$ IMEX methods in (2.9), which has been used in [31] in the analysis of the IMEX-DG method for the linear convection-diffusion equation. This method has the same implicit scheme as that of the third-order L-stable method (2.8), and their only difference is in their explicit scheme. Hence we refer to this method as an alternate L-stable method.

The explicit scheme of the alternate L-stable method, when applied to $u' = Lu$, can be written as

$$u^{n+1} = u^n + \tau L u^n + \frac{1}{2}(\tau L)^2 u^n + \frac{1}{6}(\tau L)^3 u^n + \gamma^2 a_1 a_2 (\tau L)^4 u^n.$$

Since

$$(-1)^2 \left(\gamma^2 a_1 a_2 - \frac{1}{4!} \right) > 0,$$

one can invoke [26, Theorem 4.4] to show that the explicit scheme is not strongly stable in general. See also the analysis in [8] for further discussions on the stability of the method. Indeed, it seems that we do have $\rho(K(z, \lambda, \theta)) > 1$ in the von Neumann analysis. This will force the CFL condition $\hat{\lambda}(\theta)$ to be almost zero for small θ when we use the following criterion to find $\hat{\lambda(\theta)}$ numerically

$$\sup_{z \in [0, 2\pi)} \rho(K(z, \lambda, \theta)) \leq 1 + 10^{-16}. \tag{3.3}$$

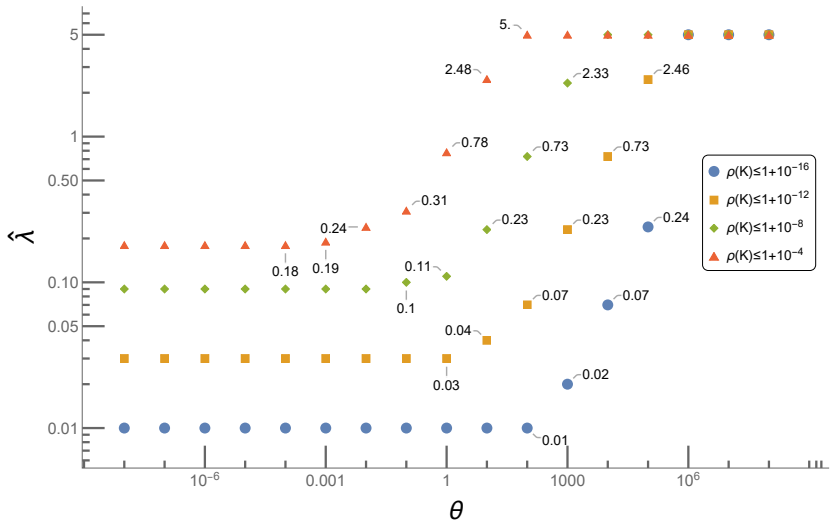

Figure 3: Relaxation of the timestep constraint for the Alternate L-stable $(3, 4, 3)$ method under different thresholds. $\hat{\lambda}$ was capped at 5.

The $\hat{\lambda} - \theta$ curve obtained through (3.3) with the DG spatial discretization is shown in Figure 3. However, if the requirement is relaxed to be

$$\sup_{z\in[0,2\pi)} \rho(K(z, \lambda, \theta)) \leq 1 + 10^{-4}, \tag{3.4}$$

we will have a larger value of the CFL constraint (see Figure 3).

Numerically, we have tested the alternate L-stable method with P^2-DG spatial discretization for the same test (3.2). It can be observed from Table 4 that the numerical scheme is stable when $\lambda = 0.18$ but becomes unstable when $\lambda = 0.19$ over coarse meshes with $10^{-6} \leq \theta \leq 6.4 \times 10^{-5}$, indicating that the actual CFL number could be $\lambda \leq \hat{\lambda} \approx 0.18$ in the tested regime. This happens to coincide with the bound obtained through the relaxed condition (3.4), which is larger than the $\hat{\lambda}$ value obtained from (3.3).

On the other hand, when $\tau = 0.18h$, although the solution doesn't blow up, the L^2 norm of the solution may still grow at the final time. This is shown in Table 4 by the values in the last column being positive. This indicates that the numerical scheme is indeed not strongly stable and may violate the condition $\rho(K) \leq 1$.

λ	N	θ	L^2 error	order	$\|u^n\|_{L^2} - \|u^0\|_{L^2}$
0.18	10	1e-06	7.8539e-03	–	4.6160e-03
	20	4e-06	9.4092e-04	3.0613	7.4548e-04
	40	1.6e-05	1.1127e-04	3.0800	9.7020e-05
	80	6.4e-05	1.3392e-05	3.0546	1.2164e-05
	160	2.56e-04	1.6372e-06	3.0320	1.5168e-06
	320	1.024e-03	2.0220e-07	3.0174	1.8918e-07
	640	4.096e-03	2.5121e-08	3.0088	2.3618e-08
0.19	10	1e-06	6.7959e+07	–	6.7959e+07
	20	4e-06	2.2363e+32	-81.4446	2.2363e+32
	40	1.6e-05	2.1989e+79	-156.1063	2.1989e+79
	80	6.4e-05	9.9955e+152	-244.6853	9.9955e+152
	160	2.56e-04	Inf	-Inf	Inf
	320	1.024e-03	2.3358e-07	Inf	2.2239e-07
	640	4.096e-03	2.9060e-08	3.0068	2.7771e-08

Table 4: Alternative L-stable method coupled with the P^2-DG method. $d = 4\pi^2 \cdot 10^{-8}$. Error table and norm increment at $T = 100$.

At last, we would like to further comment on the difference between $\hat{\lambda}_{\min}$ and $\hat{\lambda}_\infty$. For any given equation, d is fixed, hence $\theta = d/h^2$ may change as we refine the mesh (i.e., decrease h). Therefore, the maximum allowable CFL number $\hat{\lambda}(\theta)$ will also change as we refine the mesh. We again consider Table 4 with $\lambda = 0.19$. Initially, on the most coarse mesh ($N = 10$), this method is unstable, since $\lambda = 0.19$ is above the maximum allowable CFL number $\hat{\lambda}(\theta) = 0.18$ in this region. As we refine the mesh, the method first appears to be unstable for an intermediate size of h, but then becomes stable if the mesh is further refined, since θ increases to a regime where the corresponding $\tilde{\lambda}(\theta)$ becomes larger (see Table 4 and Figure 3). From this numerical example, one can see that the numerical solutions may exhibit different stability behaviors at different mesh levels. More generally, one can expect that $\hat{\lambda}_{\min}$ could serve as a safeguard for stability in all regimes and for all mesh sizes, although it could be more restrictive than what is actually needed; while if one only considers the stability as the mesh is sufficiently refined, $\hat{\lambda}_\infty$ may play a more critical role.

4 Asymptotic limits of the CFL conditions

Despite the tests with specific IMEX-RK methods in Section 3, it is natural to ask if there is a criterion for determining which IMEX-RK methods will allow large time-step size as $\theta \to \infty$. In other words, given an IMEX method, is it possible to tell whether $\hat{\lambda}_\infty > \lambda_\star > 0$ for some positive constant $\lambda_\star$?

Since $\hat{\lambda}(\theta)$ is defined through the condition $\rho\left(K(z,\lambda,\theta)\right) \le 1$, we try to investigate the relationships between $\hat{\lambda}_\infty$ and $\lim\limits_{\theta\to\infty} \rho\left(K(z,\lambda,\theta)\right) \le 1$. However, it seems to be very difficult to derive a sufficient condition for $\hat{\lambda}_\infty > \lambda_\star$. Currently, we have only succeeded in establishing a necessary condition, which can help us rule out some of the unfavorable IMEX methods. See Section 4.1 for further details. In Section 4.2, we use different $(2,2,2)$ methods to numerically investigate the relationships between $\hat{\lambda}_\infty$ and $\lim\limits_{\theta\to\infty} \rho\left(K(z,\lambda,\theta)\right) \le 1$.

4.1 Some theoretical analyses

The following theorem provides a necessary condition for $\hat{\lambda}_\infty > \lambda_\star > 0$. This theorem is derived by only using the definition of $\hat{\lambda}(\theta)$. At this moment, we don't need to specify the IMEX and the spatial discretization methods to be used.

Theorem 4.1. *Suppose $\hat{\lambda}_\infty$ and $\lim\limits_{\theta\to\infty} \rho\left(K(z,\lambda,\theta)\right)$ exist. Let $\lambda_\star > 0$ be a fixed positive constant, and we have*

$$\hat{\lambda}_\infty > \lambda_\star \quad \Longrightarrow \quad \lim_{\theta\to\infty} \rho\left(K(z,\lambda_\star,\theta)\right) \le 1, \quad \forall z \in [0,2\pi).$$

Proof. It suffices to prove the contrapositive of the statement, namely,

$$\exists z_\star \in [0,2\pi) \text{ such that } \lim_{\theta\to\infty} \rho\left(K(z_\star,\lambda_\star,\theta)\right) > 1 \quad \Longrightarrow \quad \lim_{\theta\to\infty} \hat{\lambda}(\theta) \le \lambda_\star. \tag{4.1}$$

Indeed, for the fixed $z_\star$ and $\lambda_\star$, we can find a sequence $\{\theta_i\}$ such that

$$\lim_{i\to\infty} \theta_i \to \infty \quad \text{and} \quad \rho(K(z_\star,\lambda_\star,\theta_i)) > 1 \quad \forall i.$$

Hence it follows from the definition (3.1) of $\hat{\lambda}(\cdot)$ that

$$\begin{aligned}
\hat{\lambda}(\theta_i) &= \sup\left\{\tilde{\lambda} : \rho\left(K\left(z,\lambda,\theta_i\right)\right) \le 1,\, \forall\, 0 \le z < 2\pi,\, 0 \le \lambda \le \tilde{\lambda}\right\} \\
&\le \sup\left\{\tilde{\lambda} : \rho\left(K\left(z_\star,\lambda,\theta_i\right)\right) \le 1,\, \forall\, 0 \le \lambda \le \tilde{\lambda}\right\} \\
&\le \lambda_\star.
\end{aligned}$$

Therefore, it implies $\lim\limits_{i\to\infty} \hat{\lambda}(\theta_i) \le \lambda_\star$. Since $\lim\limits_{\theta\to\infty} \hat{\lambda}(\theta)$ exists, this limit has to coincide with $\lim\limits_{i\to\infty} \hat{\lambda}(\theta_i)$, which means

$$\lim_{\theta\to\infty} \hat{\lambda}(\theta) = \lim_{i\to\infty} \hat{\lambda}(\theta_i) \le \lambda_\star.$$

□

The following theorem can be proved by using (4.1) and considering a sequence of (λ_i, z_i) with $\lambda_i \to 0$ as $i \to \infty$. It tells us when the IMEX method may perform poorly as $\theta \to \infty$.

Theorem 4.2. *Under the assumptions of Theorem 4.1, let $\lambda_0 > 0$ be a fixed constant. We have*

$$\lim_{\theta\to\infty} \rho\left(K(z,\lambda,\theta)\right) > 1,\ \forall z \in [0, 2\pi),\ \lambda \le \lambda_0 \quad \Longrightarrow \quad \hat{\lambda}_\infty = 0.$$

Below, we will discuss how to verify the condition of this theorem for various IMEX methods coupled with an FD or a DG spatial discretization. Although the analysis proceeds quite differently with an FD or a DG spatial discretization, their results share many similarities. Therefore, in the following sections, we will present our main results for both methods under the same theorems. Recall that we use the triplet (s, σ, p) to denote an s-stage implicit, σ-stage explicit, order p IMEX method with $p \ge 1$. We will analyze general IMEX methods associated with the following tableaux:

- $(2, 2, p)$ methods

$$\begin{array}{c|cc} c_1 & a_{11} & 0 \\ c_2 & a_{21} & a_{22} \\ \hline & b_1 & b_2 \end{array} \qquad \begin{array}{c|cc} \tilde{c}_1 & 0 & 0 \\ \tilde{c}_2 & \tilde{a}_{21} & 0 \\ \hline & \tilde{b}_1 & \tilde{b}_2 \end{array} \tag{4.2}$$

- $(2, 3, p)$ methods

$$\begin{array}{c|ccc} c_1 & 0 & 0 & 0 \\ c_2 & 0 & a_{22} & 0 \\ c_3 & 0 & a_{32} & a_{33} \\ \hline & 0 & b_2 & b_3 \end{array} \qquad \begin{array}{c|ccc} \tilde{c}_1 & 0 & 0 & 0 \\ \tilde{c}_2 & \tilde{a}_{21} & 0 & 0 \\ \tilde{c}_3 & \tilde{a}_{31} & \tilde{a}_{32} & 0 \\ \hline & \tilde{b}_1 & \tilde{b}_2 & \tilde{b}_3 \end{array} \tag{4.3}$$

- $(3, 3, p)$ methods

$$\begin{array}{c|ccc} c_1 & a_{11} & 0 & 0 \\ c_2 & a_{21} & a_{22} & 0 \\ c_3 & a_{31} & a_{32} & a_{33} \\ \hline & b_1 & b_2 & b_3 \end{array} \qquad \begin{array}{c|ccc} \tilde{c}_1 & 0 & 0 & 0 \\ \tilde{c}_2 & \tilde{a}_{21} & 0 & 0 \\ \tilde{c}_3 & \tilde{a}_{31} & \tilde{a}_{32} & 0 \\ \hline & \tilde{b}_1 & \tilde{b}_2 & \tilde{b}_3 \end{array}$$

- $(3, 4, p)$ methods

$$\begin{array}{c|cccc} c_1 & 0 & 0 & 0 & 0 \\ c_2 & 0 & a_{22} & 0 & 0 \\ c_3 & 0 & a_{32} & a_{33} & 0 \\ c_4 & 0 & a_{42} & a_{43} & a_{44} \\ \hline & 0 & b_2 & b_3 & b_4 \end{array} \qquad \begin{array}{c|cccc} \tilde{c}_1 & 0 & 0 & 0 & 0 \\ \tilde{c}_2 & \tilde{a}_{21} & 0 & 0 & 0 \\ \tilde{c}_3 & \tilde{a}_{31} & \tilde{a}_{32} & 0 & 0 \\ \tilde{c}_4 & \tilde{a}_{41} & \tilde{a}_{42} & \tilde{a}_{43} & 0 \\ \hline & \tilde{b}_1 & \tilde{b}_2 & \tilde{b}_3 & \tilde{b}_4 \end{array}$$

- $(4, 3, p)$ methods

$$\begin{array}{c|cccc} c_1 & a_{11} & 0 & 0 & 0 \\ c_2 & a_{21} & a_{22} & 0 & 0 \\ c_3 & a_{31} & a_{32} & a_{33} & 0 \\ c_4 & a_{41} & a_{42} & a_{43} & a_{44} \\ \hline & b_1 & b_2 & b_3 & b_4 \end{array} \qquad \begin{array}{c|cccc} \tilde{c}_1 & 0 & 0 & 0 & 0 \\ \tilde{c}_2 & 0 & 0 & 0 & 0 \\ \tilde{c}_3 & 0 & \tilde{a}_{21} & 0 & 0 \\ \tilde{c}_4 & 0 & \tilde{a}_{31} & \tilde{a}_{32} & 0 \\ \hline & 0 & \tilde{b}_2 & \tilde{b}_3 & \tilde{b}_4 \end{array}$$

Remark 4.3. *We remark that with special coefficients in the Butcher tableau, the stage number of the corresponding RK scheme can be smaller. But in this section, we still refer to these methods in the way above for convenience.*

Throughout this section, we will make the following assumptions on the diagonal coefficients a_{ii} of the implicit tableau and the dispersion operator D in (2.4).

Assumption 4.4.

- *We require $a_{ii} \neq 0$ for all i whenever the first column of the implicit method is not padded with zeros. If the first column is padded with zeros then we require $a_{ii} \neq 0$ for all $i \ge 2$.*
- *We assume $D \neq 0$ if an FD spatial discretization is used, and $\det(D) \neq 0$ if a DG discretization is used.*

Remark 4.5. *In practice, the cases of $D = 0$ or $\det(D) = 0$ need to be handled separately to check if they result in a stricter time-step restriction for satisfying $\rho(K(z, \lambda, \theta)) \le 1$. These cases typically occur when $z = \omega h$ is a multiple of 2π. Since D is 2π-periodic in z, one need only analyze the case of $z = 0$.*

The following assumption can be verified easily for the FD and P^1-DG schemes. But for the P^2-DG method, due to the complicated root formula for cubic polynomials, we state it as an assumption.

Assumption 4.6.

$$\lim_{\theta\to\infty} \rho(K(z,\lambda,\theta)) = \rho\left(\lim_{\theta\to\infty} K(z,\lambda,\theta)\right) \quad \textit{for } P^2\textit{-DG scheme.} \tag{4.4}$$

Under the above assumptions, we may obtain some unified necessary stability conditions that are independent of the method's temporal order. These conditions are also the same for any FD, P^1-, or P^2-DG spatial discretization. Hence, unless otherwise stated, our stability criteria will apply to all these spatial discretizations.

The notation [19]

$$\phi(\zeta) = \frac{\det(I - \zeta A + \zeta e b^T)}{\det(I - \zeta A)} \tag{4.5}$$

is used to represent the stability function of the implicit RK method in the IMEX scheme, defined by the coefficient matrix A and the weight vector b, with $e = [1, 1, ..., 1]^T$. Moreover, we denote by

$$\phi(-\infty) = \lim_{\zeta\to-\infty} \phi(\zeta) \tag{4.6}$$

when the limit exists. It is interesting to see that for $(2, 2, p)$, $(3, 3, p)$, and $(4, 3, p)$ IMEX methods, the necessary stability condition is independent of the explicit tableau; while for $(2, 3, p)$ and $(3, 4, p)$ methods, the explicit tableau may affect the spectral radius of K in the limit $\theta \to \infty$. These results are summarized in the subsections below.

4.1.1 Necessary stability condition for $(2, 2, p)$, $(3, 3, p)$, and $(4, 3, p)$ methods

Lemma 4.7. *Assume Assumptions 4.4 and 4.6. Consider a $(2, 2, p)$, $(3, 3, p)$, or $(4, 3, p)$ IMEX method, coupled with an arbitrary FD, a P^1-DG or a P^2-DG spatial discretization. For fixed z and λ, we have*

$$\lim_{\theta\to\infty} \rho(K(z,\lambda,\theta)) = |\phi(-\infty)|\,.$$

Note that the limit is a constant independent of z and λ.

The proof of this lemma for the $(2, 2, p)$ IMEX method coupled with an FD or a P^1-DG method is given in Appendices A.1.1 and A.2.1, respectively. We omit the proof for other cases, as they are quite lengthy and tedious.

For completeness, we list below the values of $|\phi(-\infty)|$ for the methods we discussed. These values can be easily computed through (4.5) and (4.6): for an implicit RK method defined by A, b, c with A nonsingular [19],

$$\phi(-\infty) = 1 - b^T A^{-1} e,$$

where $e = [1, 1, ..., 1]^T$.

$$|\phi_{(2,2,p)}(-\infty)| = \left|1 - \frac{b_2}{a_{22}} - \frac{b_3}{a_{33}} + \frac{a_{32}b_3}{a_{22}a_{33}}\right|,$$

$$|\phi_{(3,3,p)}(-\infty)| = \left|1 - \frac{b_2}{a_{22}} - \frac{b_3}{a_{33}} - \frac{b_4}{a_{44}} + \frac{a_{32}b_3}{a_{22}a_{33}} + \frac{a_{42}b_4}{a_{22}a_{44}} + \frac{a_{43}b_4}{a_{33}a_{44}} - \frac{a_{32}a_{43}b_4}{a_{22}a_{33}a_{44}}\right|,$$

$$\begin{aligned}|\phi_{(4,3,p)}(-\infty)| = \Bigg|1 &- \frac{b_1}{a_{11}} - \frac{b_2}{a_{22}} - \frac{b_3}{a_{33}} - \frac{b_4}{a_{44}} + \frac{a_{21}b_2}{a_{11}a_{22}} + \frac{a_{31}b_3}{a_{11}a_{33}} + \frac{a_{32}b_3}{a_{22}a_{33}} + \frac{a_{41}b_4}{a_{11}a_{44}} + \frac{a_{42}b_4}{a_{22}a_{44}} \\ &+ \frac{a_{43}b_4}{a_{33}a_{44}} - \frac{a_{21}a_{32}b_3}{a_{11}a_{22}a_{33}} - \frac{a_{21}a_{42}b_4}{a_{11}a_{22}a_{44}} - \frac{a_{31}a_{43}b_4}{a_{11}a_{33}a_{44}} - \frac{a_{32}a_{43}b_4}{a_{22}a_{33}a_{44}} + \frac{a_{21}a_{32}a_{43}b_4}{a_{11}a_{22}a_{33}a_{44}}\Bigg|.\end{aligned}$$

Combining Theorem 4.2 and Lemma 4.7, we have the following result.

Theorem 4.8. *Under the setting of Lemma 4.7, if* $|\phi(-\infty)| > 1$*, we have* $\hat{\lambda}_\infty = 0$.

Recall that for an A-stable method, we have $|\phi(\zeta)| \le 1$ for all ζ with $\mathrm{Re}(\zeta) < 0$, which implies $|\phi(-\infty)| \le 1$. As a consequence, if the IMEX method's implicit component is A-stable, it will automatically satisfy the necessary condition in Theorem 4.1, which can be summarized below:

Corollary 4.9. *Under the setting of Lemma 4.7,*

$$L\text{-stable} \Longrightarrow A\text{-stable} \Longrightarrow \lim_{\theta\to\infty} \rho(K(z,\lambda,\theta)) \le 1, \ \forall z, \lambda.$$

4.1.2 Necessary stability condition for $(2,3,p)$ and $(3,4,p)$ methods

Lemma 4.10. *Assume Assumptions 4.4 and 4.6. Consider a* $(s, s+1, p)$ *IMEX method with* $s = 2, 3$*, coupled with an arbitrary FD, a* P^1*-DG, or a* P^2*-DG spatial discretization. For fixed* z *and* λ*, we have*

$$\lim_{\theta\to\infty} \rho(K(z,\lambda,\theta)) = \max_{\kappa\in\mathrm{eig}(C(z))} \left| \, |\phi(-\infty)| + \lambda\alpha\kappa \right|. \tag{4.7}$$

Here $|\phi(-\infty)|$ *is the limit of the stability function associated with the implicit RK method of the IMEX scheme,* α *is a constant dependent on the coefficients of both explicit and implicit RK methods in the IMEX scheme, and* $C(z)$ *is the matrix for the convection operator defined in (2.4), which depends on* z *but is independent of* λ *and* θ*.*

The proof of this lemma for the $(2,3,p)$ IMEX method coupled with an FD or a P^1-DG method is given in Appendices A.1.2 and A.2.2, respectively. As before, we omit the proof for the $(3,4,p)$ methods to save space.

With some tedious computation, the values of $|\phi(-\infty)|$ and α can be obtained:

$$\begin{aligned}
|\phi_{(2,2,p)}(-\infty)| =& 1 - \frac{b_2}{a_{22}} - \frac{b_3}{a_{33}} + \frac{a_{32}b_3}{a_{22}a_{33}}, \\
\alpha_{(2,3,p)} =& \tilde{b}_1 - \frac{\tilde{a}_{21}b_2}{a_{22}} - \frac{\tilde{a}_{31}b_3}{a_{33}} + \frac{\tilde{a}_{21}a_{32}b_3}{a_{22}a_{33}}, \\
|\phi_{(3,3,p)}(-\infty)| =& 1 - \frac{b_2}{a_{22}} - \frac{b_3}{a_{33}} - \frac{b_4}{a_{44}} + \frac{a_{32}b_3}{a_{22}a_{33}} + \frac{a_{42}b_4}{a_{22}a_{44}} + \frac{a_{43}b_4}{a_{33}a_{44}} - \frac{a_{32}a_{43}b_4}{a_{22}a_{33}a_{44}}, \\
\alpha_{(3,4,p)} =& \tilde{b}_1 - \frac{\tilde{a}_{21}b_2}{a_{22}} - \frac{\tilde{a}_{31}b_3}{a_{33}} - \frac{\tilde{a}_{41}b_4}{a_{44}} + \frac{\tilde{a}_{21}a_{32}b_3}{a_{22}a_{33}} + \frac{\tilde{a}_{21}a_{42}b_4}{a_{22}a_{44}} + \frac{\tilde{a}_{31}a_{43}b_4}{a_{33}a_{44}} - \frac{\tilde{a}_{21}a_{32}a_{43}b_4}{a_{22}a_{33}a_{44}}.
\end{aligned}$$

The following theorem can be obtained after noting that $\kappa \in \mathrm{eig}(C(z))$ is bounded for all $z \in [0, 2\pi)$, considering λ to be sufficiently small in (4.7), and then invoking Theorem 4.2.

Theorem 4.11. *Under the setting of Lemma 4.10, if* $|\phi(-\infty)| > 1$*, then* $\hat{\lambda}_\infty = 0$.

Recall that for an L-stable method, we have $\phi(-\infty) = 0$. As a consequence, we have the following corollary.

Corollary 4.12. *Under the setting of Lemma 4.10, we have*

$$L\text{-stable} \Longrightarrow \lim_{\theta\to\infty} \rho\left(K(z,\lambda,\theta)\right) \le 1, \quad \forall z \in [0,2\pi), \qquad \text{if } \lambda \le \left(|\alpha_{(s,s+1,p)}| \max_{z\in[0,2\pi)} \mathrm{eig}(C(z)) \right)^{-1}.$$

4.2 Numerical investigations with $(2,2,2)$ IMEX methods

In this section, we aim to investigate the converse of Theorem 4.1, and more generally, whether $\lim_{\theta\to\infty} \rho(K(z,\lambda,\theta)) \le 1$ will give us any information on the value of $\hat{\lambda}_\infty$.

To this end, we focus on the simplest $(2,2,2)$ IMEX methods, coupled with a P^1-DG spatial discretization. Under this setting, $\lim_{\theta\to\infty} \rho(K(z,\lambda,\theta)) = |\phi(-\infty)|$ is independent of λ according to Lemma 4.7. We have constructed many $(2,2,2)$ IMEX methods, and present a selection of them, with varying values of $|\phi(-\infty)|$, in Tableaux (4.8) through (4.13).

Tableau 1

$$\begin{array}{c|cc} 1/4 & 1/4 & 0 \\ 5/8 & -3/8 & 1 \\ \hline & 1/3 & 2/3 \end{array} \qquad \begin{array}{c|cc} 0 & 0 & 0 \\ 3/4 & 3/4 & 0 \\ \hline & 1/3 & 2/3 \end{array} \tag{4.8}$$

Tableau 2

$$\begin{array}{c|cc} 1/6 & 1/6 & 0 \\ 7/6 & 5/6 & 1/3 \\ \hline & 2/3 & 1/3 \end{array} \qquad \begin{array}{c|cc} 0 & 0 & 0 \\ 3/2 & 3/2 & 0 \\ \hline & 2/3 & 1/3 \end{array} \tag{4.9}$$

Tableau 3

$$\begin{array}{c|cc} -1/4 & -1/4 & 0 \\ 13/20 & -1/10 & 3/4 \\ \hline & 1/6 & 5/6 \end{array} \qquad \begin{array}{c|cc} 0 & 0 & 0 \\ 3/5 & 3/5 & 0 \\ \hline & 1/6 & 5/6 \end{array} \tag{4.10}$$

Tableau 4

$$\begin{array}{c|cc} 1/3 & 1/3 & 0 \\ 1/2 & 0 & 1/2 \\ \hline & 0 & 1 \end{array} \qquad \begin{array}{c|cc} 0 & 0 & 0 \\ 1/2 & 1/2 & 0 \\ \hline & 0 & 1 \end{array} \tag{4.11}$$

Tableau 5

$$\begin{array}{c|cc} 2/5 & 2/5 & 0 \\ 11/20 & 7/20 & 1/5 \\ \hline & 1/3 & 2/3 \end{array} \qquad \begin{array}{c|cc} 0 & 0 & 0 \\ 3/4 & 3/4 & 0 \\ \hline & 1/3 & 2/3 \end{array} \tag{4.12}$$

Tableau 6

$$\begin{array}{c|cc} 1/3 & 1/3 & 0 \\ 1/2 & 1/4 & 1/4 \\ \hline & 0 & 1 \end{array} \qquad \begin{array}{c|cc} 0 & 0 & 0 \\ 1/2 & 1/2 & 0 \\ \hline & 0 & 1 \end{array} \tag{4.13}$$

	A-stable	$\lvert\phi(-\infty)\rvert$	$\hat{\lambda}_\infty$	$\hat{\lambda}_{\min}$
Tableau 1	✗	> 1	0	0
Tableau 2	✓	1	1/3	1/3
Tableau 3	✗	1	0	0
Tableau 4	✓	1	0	0
Tableau 5	✓	< 1	∞	1/3
Tableau 6	✓	0	∞	1/3

Table 5: Summary of the time-step constraints for several $(2, 2, 2)$ IMEX methods.

For these $(2, 2, 2)$ IMEX methods, we compute their $\hat{\lambda} - \theta$ curve numerically via spectral analysis and report them in Figure 4. These results are also summarized in Table 5, from which we have the following observations:

- Tableau 1 is an example for validating the contrapositive of Theorem 4.1 (or Theorem 4.11), i.e., if $|\phi(-\infty)| > 1$, then $\hat{\lambda}_\infty = 0$.
- From Tableaux 2, 3, and 4 with $|\phi(-\infty)| = 1$, the limit $\hat{\lambda}_\infty$ could be either 0 or a positive constant. Hence the converse of the statement in Theorem 4.1 does not hold.
- For both Tableaux 5 and 6 with $|\phi(-\infty)| < 1$, we have $\hat{\lambda}_\infty = \infty$. Indeed, in our tests (and possibly beyond the $(2, 2, 2)$ methods), we usually observe $\hat{\lambda}_\infty > 0$ when $|\phi(-\infty)| < 1$. However,

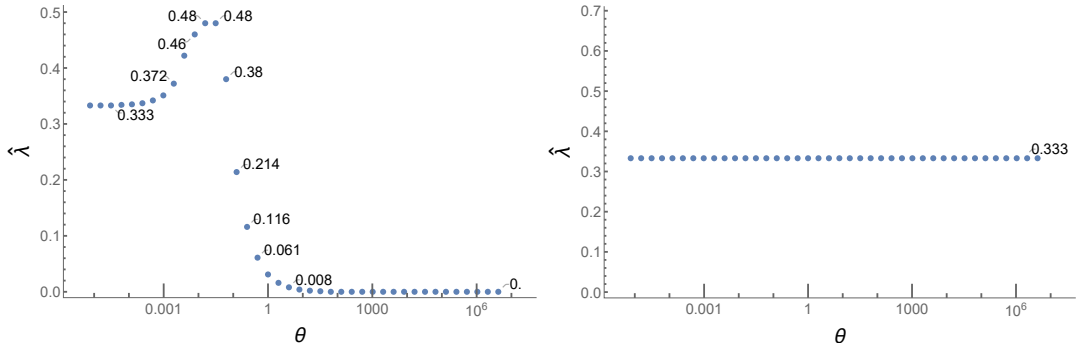

(a) Tableau 1

(b) Tableau 2

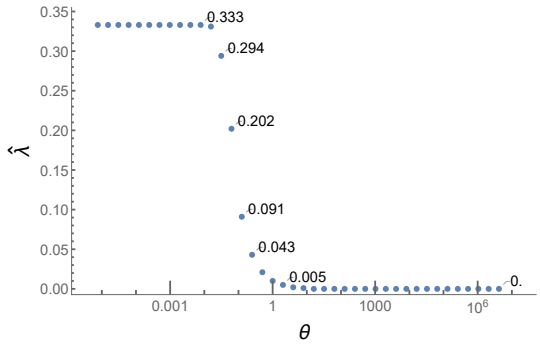

(c) Tableau 3

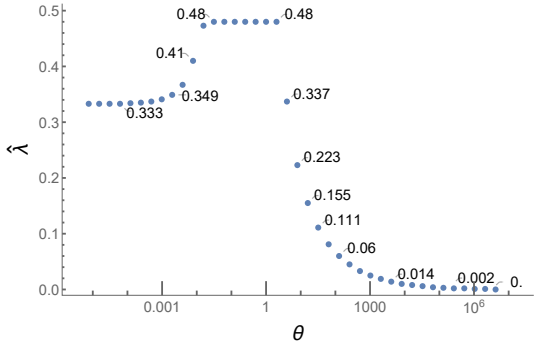

(d) Tableau 4

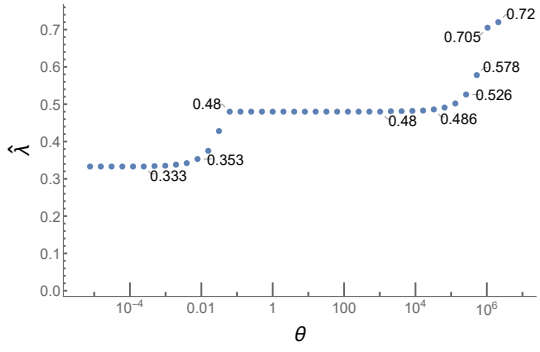

(e) Tableau 5

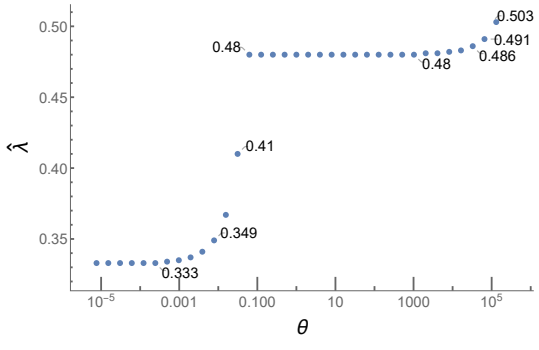

(f) Tableau 6

Figure 4: $\hat{\lambda} - \theta$ curve for each of the six methods in Table 5 using P^1-DG methods. *Note: values displayed as zero may not be zero, but strictly less than* 10^{-3}.

we are unable to provide rigorous proof, and the complication lies in that we may not be able to interchange lim and sup when evaluating

$$\lim_{\theta\to\infty} \hat{\lambda}(\theta) = \lim_{\theta\to\infty} \sup \left\{ \tilde{\lambda} : \rho\left(K\left(z, \lambda, \theta\right)\right) \leq 1, \, \forall\, 0 \leq z < 2\pi, \, 0 \leq \lambda \leq \tilde{\lambda} \right\}.$$

- A-stability of the implicit component of the IMEX method is not always a safeguard for good performance in the limit as $\theta \to \infty$. Indeed, we may have $\hat{\lambda}_\infty = 0$ even if the implicit scheme of the IMEX method is A-stable. Tableau 4 provides an example of this case.

5 Conclusions

In this paper, we have studied the stability and time-step constraints for solving the linearized KdV equation using IMEX-RK time integration methods. Both FD and DG spatial discretizations have been considered. Using the Fourier method, we investigate the CFL number for several IMEX-RK methods to understand how it changes as a function of $\theta = d/h^2$, and demonstrate that some IMEX methods may have better stability properties. We also investigated the asymptotic behavior of the CFL number as $\theta \to \infty$ and derived a necessary condition for such a limit to be positive. Some numerical tests are provided to illustrate the performance of IMEX DG methods under different time-step constraints.

Acknowledgments

The work of Z. Sun is partially supported by the NSF grant DMS-2208391. The work of Y. Xing is partially sponsored by the NSF grant DMS-1753581.

Statements and Declarations

This work was partially supported by the NSF grants. Y. Xing serves as an Associate Editor of the journal "Communications on Applied Mathematics and Computation". On behalf of all authors, the corresponding author states that there is no conflict of interest.

References

[1] G. Akrivis, M. Crouzeix, and C. Makridakis. Implicit-explicit multistep finite element methods for nonlinear parabolic problems. *Mathematics of Computation*, 67(222):457–477, 1998.

[2] G. Akrivis, M. Crouzeix, and C. Makridakis. Implicit-explicit multistep methods for quasilinear parabolic equations. *Numerische Mathematik*, 82:521–541, 1999.

[3] U. M. Ascher, S. J. Ruuth, and R. J. Spiteri. Implicit-explicit Runge-Kutta methods for time-dependent partial differential equations. *Applied Numerical Mathematics*, 25(2-3):151–167, 1997.

[4] U. M. Ascher, S. J. Ruuth, and B. T. Wetton. Implicit-explicit methods for time-dependent partial differential equations. *SIAM Journal on Numerical Analysis*, 32(3):797–823, 1995.

[5] F. Bassi and S. Rebay. A high-order accurate discontinuous finite element method for the numerical solution of the compressible Navier–Stokes equations. *Journal of computational physics*, 131(2):267–279, 1997.

[6] J. L. Bona, H. Chen, O. A. Karakashian, and Y. Xing. Conservative, discontinuous Galerkin-methods for the Generalized Korteweg-de Vries equation. *Mathematics of Computation*, 82:1401–1432, 2013.

[7] S. Boscarino, L. Pareschi, and G. Russo. Implicit-explicit Runge–Kutta schemes for hyperbolic systems and kinetic equations in the diffusion limit. *SIAM Journal on Scientific Computing*, 35(1):A22–A51, 2013.

[8] M. Calvo, J. De Frutos, and J. Novo. Linearly implicit Runge–Kutta methods for advection–reaction–diffusion equations. *Applied Numerical Mathematics*, 37(4):535–549, 2001.

[9] Y. Cheng, C.-S. Chou, F. Li, and Y. Xing. L^2 stable discontinuous Galerkin methods for one-dimensional two-way wave equations. *Mathematics of Computation*, 86:121–155, 2017.

[10] N. Chuenjarern and Y. Yang. Fourier analysis of local discontinuous Galerkin methods for linear parabolic equations on overlapping meshes. *Journal of Scientific Computing*, 81:671–688, 2019.

[11] B. Cockburn and C.-W. Shu. The local discontinuous Galerkin method for time-dependent convection-diffusion systems. *SIAM Journal on Numerical Analysis*, 35(6):2440–2463, 1998.

[12] B. Cockburn and C.-W. Shu. Runge–Kutta discontinuous Galerkin methods for convection-dominated problems. *Journal of Scientific Computing*, 16(3):173–261, 2001.

[13] M. Dehghan and M. Abbaszadeh. Variational multiscale element free Galerkin (VMEFG) and local discontinuous Galerkin (LDG) methods for solving two-dimensional Brusselator reaction–diffusion system with and without cross-diffusion. *Computer Methods in Applied Mechanics and Engineering*, 300:770–797, 2016.

[14] W. Deng and J. S. Hesthaven. Local discontinuous Galerkin methods for fractional diffusion equations. *ESAIM: Mathematical Modelling and Numerical Analysis-Modélisation Mathématique et Analyse Numérique*, 47(6):1845–1864, 2013.

[15] D. Dutykh, T. Katsaounis, and D. Mitsotakis. Finite volume methods for unidirectional dispersive wave models. *International Journal for Numerical Methods in Fluids*, 71(6):717–736, 2013.

[16] D. J. Frean and J. K. Ryan. Superconvergence and the numerical flux: A study using the upwind-biased flux in discontinuous Galerkin methods. *Communications on Applied Mathematics and Computation*, 2(3):461–486, 2020.

[17] S. Gottlieb, Z. J. Grant, J. Hu, and R. Shu. High order strong stability preserving multiderivative implicit and IMEX Runge–Kutta methods with asymptotic preserving properties. *SIAM Journal on Numerical Analysis*, 60(1):423–449, 2022.

[18] W. Guo, X. Zhong, and J.-M. Qiu. Superconvergence of discontinuous Galerkin and local discontinuous Galerkin methods: eigen-structure analysis based on Fourier approach. *Journal of Computational Physics*, 235:458–485, 2013.

[19] E. Hairer and G. Wanner. *Stability Function of Implicit RK-Methods*, pages 40–50. Springer Berlin Heidelberg, Berlin, Heidelberg, 1996.

[20] C. Hufford and Y. Xing. Superconvergence of the local discontinuous Galerkin method for the linearized Korteweg-de Vries equation. *Journal of Computational and Applied Mathematics*, 255:441–455, 2014.

[21] A. Kanevsky, M. H. Carpenter, D. Gottlieb, and J. S. Hesthaven. Application of implicit–explicit high order Runge–Kutta methods to discontinuous-Galerkin schemes. *Journal of Computational Physics*, 225(2):1753–1781, 2007.

[22] X. Li, Y. Xing, and C.-S. Chou. Optimal energy conserving and energy dissipative local discontinuous Galerkin methods for the Benjamin-Bona-Mahony equation. *Journal of Scientific Computing*, 83:17, 2020.

[23] Y. Li, C.-W. Shu, and S. Tang. A local discontinuous Galerkin method for nonlinear parabolic SPDEs. *ESAIM: Mathematical Modelling and Numerical Analysis*, 55:S187–S223, 2021.

[24] L. Pareschi and G. Russo. Implicit–explicit Runge–Kutta schemes and applications to hyperbolic systems with relaxation. *Journal of Scientific computing*, 25:129–155, 2005.

[25] J. Sun, S. Xie, and Y. Xing. Local discontinuous Galerkin methods for the nonlinear abcd-Boussinesq system. *Communications on Applied Mathematics and Computation*, 4:381–416, 2022.

[26] Z. Sun and C.-W. Shu. Strong stability of explicit Runge–Kutta time discretizations. *SIAM Journal on Numerical Analysis*, 57(3):1158–1182, 2019.

[27] Z. Sun and Y. Xing. On structure-preserving discontinuous Galerkin methods for Hamiltonian partial differential equations: energy conservation and multi-symplecticity. *Journal of Computational Physics*, 419:109662, 2020.

[28] M. Tan, J. Cheng, and C.-W. Shu. Stability of high order finite difference schemes with implicit-explicit time-marching for convection-diffusion and convection-dispersion equations. *International Journal of Numerical Analysis and Modeling*, 18(3):362–383, 2021.

[29] M. Tan, J. Cheng, and C.-W. Shu. Stability of high order finite difference and local discontinuous Galerkin schemes with explicit-implicit-null time-marching for high order dissipative and dispersive equations. *Journal of Computational Physics*, 464:111314, 2022.

[30] L. Tian, Y. Xu, J. G. Kuerten, and J. J. van der Vegt. An h-adaptive local discontinuous Galerkin method for the Navier–Stokes–Korteweg equations. *Journal of computational physics*, 319:242–265, 2016.

[31] H. Wang, C.-W. Shu, and Q. Zhang. Stability and error estimates of local discontinuous Galerkin methods with implicit-explicit time-marching for advection-diffusion problems. *SIAM Journal on Numerical Analysis*, 53(1):206–227, 2015.

[32] Y. Xu and C.-W. Shu. Local discontinuous Galerkin methods for high-order time-dependent partial differential equations. *Communications in Computational Physics*, 7(1):1, 2010.

[33] J. Yan and C.-W. Shu. A local discontinuous Galerkin method for KdV type equations. *SIAM Journal on Numerical Analysis*, 40(2):769–791, 2002.

[34] H. Yang, F. Li, and J. Qiu. Dispersion and dissipation errors of two fully discrete discontinuous Galerkin methods. *Journal of Scientific Computing*, 55(3):552–574, 2013.

[35] M. Zhang and C.-W. Shu. An analysis of three different formulations of the discontinuous Galerkin method for diffusion equations. *Mathematical Models and Methods in Applied Sciences*, 13(03):395–413, 2003.

[36] X. Zhong and C.-W. Shu. Numerical resolution of discontinuous Galerkin methods for time dependent wave equations. *Computer Methods in Applied Mechanics and Engineering*, 200(41-44):2814–2827, 2011.

A Proof of Lemma 4.7 and 4.10 in the simple case

In this Appendix, we consider $(2,2,p)$ and $(2,3,p)$ IMEX methods coupled with an FD or a P^1-DG spatial discretization. We will prove Lemma 4.7 for the $(2,2,p)$ method in both cases and extend the proof to prove Lemma 4.10 for the $(2,3,p)$ method. Our analysis further enables us to adapt these proofs for $(3,3,p)$, $(4,3,p)$, and $(3,4,p)$ methods when combined with FD discretizations. For P^2-DG discretizations, the analysis becomes considerably more challenging, and we have checked both lemmas hold under the continuity assumption

$$\lim_{\theta\to\infty} \rho(K) = \rho(\lim_{\theta\to\infty} K),$$

using the software Mathematica.

Recall the tableaux for $(2,2,p)$ and $(2,3,p)$ methods take the form (4.2) and (4.3). We will discuss the case with an FD or a P^1-DG spatial discretization separately.

A.1 Spectral Analysis with FD spatial discretization

A.1.1 Proof of Lemma 4.7 with a $(2,2,p)$ method coupled with FD

We first consider a $(2,2,p)$ method, and aim to prove Lemma 4.7. When using an FD discretization, C and D from (2.4) are scalars that depend on $z = \omega h$. Applying the IMEX method (4.2) to (2.4) yields the following stage equations after rearranging terms:

$$\hat{u}^{n,1} = K_1 \hat{u}^n, \qquad \hat{u}^{n,2} = K_2 \hat{u}^n, \qquad \hat{u}^{n+1} = K \hat{u}^n,$$

where K_1, K_2 and K are given by

$$K_1 = M_{11}, \tag{A.1a}$$
$$K_2 = M_{22}(1 + \lambda \tilde{a}_{21} C K_1 + \lambda \theta a_{21} D K_1), \tag{A.1b}$$
$$K = 1 + \lambda \tilde{b}_1 C K_1 + \lambda b_1 D(\theta K_1) + \lambda \tilde{b}_2 C K_2 + \lambda b_2 D(\theta K_2), \tag{A.1c}$$
$$M_{ii} = (1 - \lambda \theta a_{ii} D)^{-1}, \qquad i = 1, 2. \tag{A.1d}$$

The goal is to show for fixed λ and z

$$\lim_{\theta \to \infty} \rho(K) = \lim_{\theta \to \infty} |K| = \left| \lim_{\theta \to \infty} K \right| = \left| 1 - \frac{b_1}{a_{11}} - \frac{b_2}{a_{22}} + \frac{a_{21} b_2}{a_{11} a_{22}} \right|. \tag{A.2}$$

Since K is a scalar, the first two equalities are obvious, and we focus on showing the last equality by evaluating the limit of K. For fixed λ and z, we observe that C and D do not depend on θ, and that both K_1 and K_2 are rational functions of the variable θ. When $\theta \to \infty$, it is easy to observe that $M_{ii} = O(1/\theta)$. Therefore, K_1 is at the level of $O(1/\theta)$ and K_2 is at the level of $O(1/\theta + 1/\theta^2)$, which leads to

$$\lim_{\theta \to \infty} 1 + \lambda \tilde{b}_1 C K_1 + \lambda \tilde{b}_2 C K_2 = 1.$$

In addition, we have

$$\lim_{\theta \to \infty} \lambda b_1 D(\theta K_1) = \lim_{\theta \to \infty} \frac{\lambda b_1 D \theta}{1 - \lambda \theta a_{11} D} = \frac{\lambda b_1 D}{-\lambda a_{11} D} = -\frac{b_1}{a_{11}}.$$

Following a similar analysis leads to the limit of the last term

$$\begin{aligned} \lim_{\theta \to \infty} \lambda b_2 D(\theta K_2) &= \lim_{\theta \to \infty} \frac{\lambda b_2 D \theta (1 - \lambda \theta a_{11} D + \lambda \tilde{a}_{21} C + \lambda \theta a_{21} D)}{(1 - \lambda \theta a_{11} D)(1 - \lambda \theta a_{22} D)} \\ &= \frac{-\lambda^2 a_{11} b_2 D^2 + \lambda^2 a_{21} b_2 D^2}{\lambda^2 a_{11} a_{22} D^2} = -\frac{b_2}{a_{22}} + \frac{a_{21} b_2}{a_{11} a_{22}}. \end{aligned}$$

Combining all these results yields

$$\left| \lim_{\theta \to \infty} K \right| = \left| 1 - \frac{b_1}{a_{11}} - \frac{b_2}{a_{22}} + \frac{a_{21} b_2}{a_{11} a_{22}} \right|,$$

which finishes the proof of (A.2). The same analysis can be extended to prove Lemma 4.7 for $(3,3,p)$ and $(4,3,p)$ IMEX methods coupled with an FD discretization. We omit these details for brevity.

A.1.2 Proof of Lemma 4.10 with a $(2,3,p)$ method coupled with FD

Next, we consider a $(2,3,p)$ method (4.3), and aim to prove Lemma 4.10 by adapting the above proof. Applying this method to (2.4) yields the same definition of M_{ii} but with K_1, K_2, and K defined as

$$K_1 = M_{22}(1 + \lambda \tilde{a}_{21} C), \tag{A.3a}$$
$$K_2 = M_{33}(1 + \lambda \tilde{a}_{31} C + \lambda \tilde{a}_{32} C K_1 + \lambda \theta a_{32} D K_1), \tag{A.3b}$$
$$K = 1 + \lambda \tilde{b}_1 C + \lambda \tilde{b}_2 C K_1 + \lambda b_2 D(\theta K_1) + \lambda \tilde{b}_3 C K_2 + \lambda b_3 D(\theta K_2). \tag{A.3c}$$

The goal is to show for fixed λ and z

$$\lim_{\theta \to \infty} \rho(K) = \lim_{\theta \to \infty} |K| = \left| \lim_{\theta \to \infty} K \right| = \left| 1 - \frac{b_2}{a_{22}} - \frac{b_3}{a_{33}} + \frac{a_{32} b_3}{a_{22} a_{33}} + \lambda \alpha C \right|, \tag{A.4}$$

where

$$\alpha = \tilde{b}_1 - \frac{\tilde{a}_{21}b_2}{a_{22}} - \frac{\tilde{a}_{31}b_3}{a_{33}} + \frac{\tilde{a}_{21}a_{32}b_3}{a_{22}a_{33}}. \tag{A.5}$$

Following the same analysis as before, we observe that both K_1 and K_2 are at the level of $O(1/\theta)$, and

$$\lim_{\theta\to\infty} 1 + \lambda\tilde{b}_1 C + \lambda\tilde{b}_2 C K_1 + \lambda\tilde{b}_3 C K_2 = 1 + \lambda\tilde{b}_1 C.$$

Similarly, we have

$$\begin{aligned}
\lim_{\theta\to\infty} \lambda b_2 D(\theta K_1) &= \lim_{\theta\to\infty} \frac{\lambda\theta b_2(1+\lambda\tilde{a}_{21}C)D}{1-\lambda\theta a_{22}D} = \frac{-b_2(1+\lambda\tilde{a}_{21}C)}{a_{22}} = \frac{-b_2}{a_{22}} + \lambda\left(\frac{-\tilde{a}_{21}b_2}{a_{22}}\right)C, \\
\lim_{\theta\to\infty} \lambda b_3 D(\theta K_2) &= \frac{\lambda b_3(1+\lambda\tilde{a}_{31}C)D}{-\lambda a_{33}D} + \frac{\lambda^2 b_3 a_{32}(1+\lambda\tilde{a}_{21}C)D^2}{\lambda^2 a_{22}a_{33}D^2} \\
&= \frac{-b_3(1+\lambda\tilde{a}_{31}C)}{a_{33}} + \frac{b_3 a_{32}(1+\lambda\tilde{a}_{21}C)}{a_{22}a_{33}} \\
&= \frac{-b_3}{a_{33}} + \frac{a_{32}b_3}{a_{22}a_{33}} + \lambda\left(\frac{-\tilde{a}_{31}b_3}{a_{33}} + \frac{\tilde{a}_{21}a_{32}b_3}{a_{22}a_{33}}\right)C.
\end{aligned}$$

Therefore, combining all these analyses yields

$$\left|\lim_{\theta\to\infty} K\right| = \left|1 - \frac{b_2}{a_{22}} - \frac{b_3}{a_{33}} + \frac{a_{32}b_3}{a_{22}a_{33}} + \lambda\left(\tilde{b}_1 - \frac{\tilde{a}_{21}b_2}{a_{22}} - \frac{\tilde{a}_{31}b_3}{a_{33}} + \frac{\tilde{a}_{21}a_{32}b_3}{a_{22}a_{33}}\right)C\right|.$$

which finishes the proof of (A.4). Again, the same analysis can be extended to prove Lemma 4.10 for $(3,4,p)$ IMEX methods coupled with an FD discretization, which is omitted for brevity.

A.2 Spectral Analysis with P^1-DG spatial discretization

A.2.1 Proof of Lemma 4.7 with a $(2,2,p)$ method coupled with P^1-DG

Next, we will prove Lemma 4.7 for a $(2,2,p)$ IMEX method with a P^1-DG discretization. Now, C and D from (2.4) become matrices depending on $z = \omega h$, and we denote

$$C = \begin{bmatrix} c_{11} & c_{12} \\ c_{21} & c_{22} \end{bmatrix}, \qquad D = \begin{bmatrix} d_{11} & d_{12} \\ d_{21} & d_{22} \end{bmatrix}.$$

Applying the IMEX method (4.2) to (2.4) yields the following stage equations after rearranging terms:

$$\hat{u}^{n,1} = K_1\hat{u}^n, \qquad \hat{u}^{n,2} = K_2\hat{u}^n, \qquad \hat{u}^{n+1} = K\hat{u}^n, \tag{A.6}$$

where K_1, K_2 and K are given by (A.1a)-(A.1c), and

$$M_{ii} = (I - \lambda\theta a_{ii}D)^{-1} = \frac{1}{\gamma_{ii}}\begin{bmatrix} 1-\lambda\theta a_{ii}d_{22} & \lambda\theta a_{ii}d_{12} \\ \lambda\theta a_{ii}d_{21} & 1-\lambda\theta a_{ii}d_{11} \end{bmatrix} = \frac{1}{\gamma_{ii}}\left(I - \lambda\theta a_{ii}\det(D)D^{-1}\right), \tag{A.7}$$

with $\gamma_{ii} = (\lambda\theta a_{ii})^2\det(D) - (\lambda\theta)\mathrm{tr}(D) + 1$. The goal is to show for fixed λ and z

$$\lim_{\theta\to\infty}\rho(K) = \rho(\lim_{\theta\to\infty} K) = \left|1 - \frac{b_1}{a_{11}} - \frac{b_2}{a_{22}} + \frac{a_{21}b_2}{a_{11}a_{22}}\right|. \tag{A.8}$$

To prove the first equality of (A.8), namely, the continuity of $\rho(K)$ with respect to θ, we assume the matrix K is a 2×2 matrix with entries $k_{11}, k_{12}, k_{21}, k_{22}$. Its spectral radius $\rho(K)$ is given by

$$\rho(K) = \max\left\{\left|\frac{(k_{11}+k_{22}) \pm \sqrt{(k_{11}+k_{22})^2 - 4(k_{11}k_{22}-k_{12}k_{21})}}{2}\right|\right\}.$$

Supposing the limit of K exists (as will be shown later), we have

$$\begin{aligned}
\lim_{\theta\to\infty}\rho(K) &= \lim_{\theta\to\infty}\max\left\{\left|\frac{(k_{11}+k_{22}) \pm \sqrt{(k_{11}+k_{22})^2 - 4(k_{11}k_{22}-k_{12}k_{21})}}{2}\right|\right\} \\
&= \max\left\{\left|\lim_{\theta\to\infty}\frac{(k_{11}+k_{22}) \pm \sqrt{(k_{11}+k_{22})^2 - 4(k_{11}k_{22}-k_{12}k_{21})}}{2}\right|\right\} = \rho(\lim_{\theta\to\infty} K).
\end{aligned}$$

Now it suffices to determine the limit of K. To simplify the calculation, we first evaluate limits of K_1, θK_1, K_2, and θK_2. It can be shown that

$$\begin{aligned}\lim_{\theta\to\infty} K_1 &= \lim_{\theta\to\infty} M_{11} = \lim_{\theta\to\infty} \frac{1}{\gamma_{11}} \left(I - \lambda\theta a_{11}\det(D)D^{-1}\right) \\ &= \lim_{\theta\to\infty} \frac{I - \lambda\theta a_{11}\det(D)D^{-1}}{(\lambda\theta a_{11})^2\det(D) - (\lambda\theta)\mathrm{tr}(D) + 1} = 0, \end{aligned} \tag{A.9}$$

$$\begin{aligned}\lim_{\theta\to\infty} \theta K_1 &= \lim_{\theta\to\infty} \theta M_{11} = \lim_{\theta\to\infty} \frac{\theta}{\gamma_{11}}(I - \lambda\theta a_{11}\det(D)D^{-1}) \\ &= \lim_{\theta\to\infty} \frac{\theta I - \lambda\theta^2 a_{11}\det(D)D^{-1}}{(\lambda\theta a_{11})^2\det(D) - (\lambda\theta)\mathrm{tr}(D) + 1} = \frac{-D^{-1}}{\lambda a_{11}}. \end{aligned} \tag{A.10}$$

To compute the limit of K_2, we will consider the limits of its three terms, M_{22}, $\lambda\tilde{a}_{21}M_{22}CK_1$, and $\lambda a_{21}M_{22}D\theta K_1$ separately. The limit of the first term can be computed similarly to that of K_1:

$$\lim_{\theta\to\infty} M_{22} = \lim_{\theta\to\infty} \frac{1}{\gamma_{22}}(I - \lambda\theta a_{22}\det(D)D^{-1}) = 0.$$

For the second term, we have

$$\lim_{\theta\to\infty} \lambda\tilde{a}_{21}M_{22}CK_1 = \lambda\tilde{a}_{21} \lim_{\theta\to\infty} \frac{1}{\gamma_{11}\gamma_{22}}(I - \lambda\theta a_{22}\det(D)D^{-1})C(I - \lambda\theta a_{11}\det(D)D^{-1}) = 0,$$

since the highest-order term in the numerator is at the level of $O(\theta^2)$ and that $\gamma_{11}\gamma_{22}$ is at the level of $O(\theta^4)$. Similarly, we have

$$\lim_{\theta\to\infty} \lambda a_{21}M_{22}D\theta K_1 = \lambda a_{21} \lim_{\theta\to\infty} \frac{1}{\gamma_{11}\gamma_{22}}(I - \lambda\theta a_{22}\det(D)D^{-1})(\theta D - \lambda\theta^2 a_{11}\det(D)I) = 0,$$

since the highest-order term in the numerator is at the level of $O(\theta^3)$. Putting these three limits together leads to

$$\lim_{\theta\to\infty} K_2 = 0. \tag{A.11}$$

To determine the limit of θK_2, we can once again analyze its three terms separately. Based on our previous analysis, we can obtain

$$\begin{aligned}&\lim_{\theta\to\infty} \theta M_{22} = \frac{-D^{-1}}{\lambda a_{22}}, \qquad \lim_{\theta\to\infty} \lambda\tilde{a}_{21}M_{22}C\theta K_1 = 0, \\ &\lim_{\theta\to\infty} \lambda a_{21}M_{22}D\theta^2 K_1 = \frac{\lambda^3 a_{21}a_{11}a_{22}\det(D)^2 D^{-1}}{\lambda^4(a_{11}a_{22}\det(D))^2} = \frac{a_{21}D^{-1}}{\lambda a_{11}a_{22}}. \end{aligned}$$

Collecting all three limits together yields

$$\lim_{\theta\to\infty} \theta K_2 = \left(\frac{-1}{\lambda a_{22}} + \frac{a_{21}}{\lambda a_{11}a_{22}}\right) D^{-1}.$$

Since C and D are independent of θ, using the limits of K_1, θK_1, K_2, and θK_2 leads to

$$\begin{aligned}\lim_{\theta\to\infty} K &= \lim_{\theta\to\infty} I + \lambda\tilde{b}_1 CK_1 + \lambda b_1 D(\theta K_1) + \lambda\tilde{b}_2 CK_2 + \lambda b_2 D(\theta K_2) \\ &= I + 0 + \lambda b_1 D\frac{-D^{-1}}{\lambda a_{11}} + 0 + \lambda b_2 D\left(\frac{-1}{\lambda a_{22}} + \frac{a_{21}}{\lambda a_{11}a_{22}}\right) D^{-1} \\ &= \left(1 - \frac{b_1}{a_{11}} - \frac{b_2}{a_{22}} + \frac{b_2 a_{21}}{a_{11}a_{22}}\right) I, \end{aligned}$$

which finishes the proof of (A.8), after utilizing the continuity assumption (4.4).

A.2.2 Proof of Lemma 4.10 with a $(2,3,p)$ method coupled with P^1-DG

In the end, we consider a $(2,3,p)$ method (4.3) with a P^1-DG discretization, and aim to prove Lemma 4.10 by adapting the above proof. Applying this method to (2.4) yields the same stage equations (A.6), with K_1, K_2, and K defined in (A.3) and M_{ii} defined in (A.7). The goal is to show for fixed λ and z

$$\lim_{\theta\to\infty}\rho(K)=\rho(\lim_{\theta\to\infty}K)=\max_{\kappa\in\mathrm{eig}(C(z))}\left|1-\frac{b_2}{a_{22}}-\frac{b_3}{a_{33}}+\frac{a_{32}b_3}{a_{22}a_{33}}+\lambda\alpha\kappa\right|, \tag{A.12}$$

with α defined in (A.5).

The continuity of $\rho(K)$ in θ can be verified as that in the previous section. To validate the second equality in (A.12), we compute the limits of $K_1, \theta K_1, K_2, \theta K_2$ separately. Following the analysis in (A.9), we have

$$\lim_{\theta\to\infty}K_1=\left(\lim_{\theta\to\infty}M_{22}\right)(I+\lambda\tilde{a}_{21}C)=0.$$

Similarly, (A.10) leads to

$$\lim_{\theta\to\infty}\theta K_1=\left(\lim_{\theta\to\infty}\theta M_{22}\right)(I+\lambda\tilde{a}_{21}C)=\frac{-D^{-1}}{\lambda a_{22}}(I+\lambda\tilde{a}_{21}C).$$

We again determine the limit of K_2 by considering the limits of three terms separately. Following the same analysis in deriving (A.11), we have

$$\lim_{\theta\to\infty}K_2=0.$$

To determine the limit of θK_2, we can once again analyze its three terms separately. Using the results from the previous analysis, we can obtain

$$\begin{aligned}
\lim_{\theta\to\infty}\theta M_{33}(I+\lambda\tilde{a}_{31}C)&=\left(\lim_{\theta\to\infty}\theta M_{33}\right)(I+\lambda\tilde{a}_{31}C)=\frac{-D^{-1}}{\lambda a_{33}}(I+\lambda\tilde{a}_{31}C),\\
\lim_{\theta\to\infty}\lambda\tilde{a}_{32}\theta M_{33}CK_1&=\lambda\tilde{a}_{32}\left(\lim_{\theta\to\infty}M_{33}C\theta M_{22}\right)(I+\lambda\tilde{a}_{21}C)=0,\\
\lim_{\theta\to\infty}\lambda\theta^2 a_{32}M_{33}DK_1&=\lambda a_{32}\left(\lim_{\theta\to\infty}M_{33}D\theta^2M_{22}\right)(I+\lambda\tilde{a}_{21}C)=\frac{a_{32}D^{-1}}{\lambda a_{22}a_{33}}(I+\lambda\tilde{a}_{21}C).
\end{aligned}$$

Collecting all three limits together yields

$$\lim_{\theta\to\infty}\theta K_2=\frac{-D^{-1}}{\lambda a_{33}}(I+\lambda\tilde{a}_{31}C)+\frac{a_{32}D^{-1}}{\lambda a_{22}a_{33}}(I+\lambda\tilde{a}_{21}C).$$

Since C and D are independent of θ, using the limits of K_1, θK_1, K_2, and θK_2 leads to

$$\begin{aligned}
\lim_{\theta\to\infty}K&=\lim_{\theta\to\infty}I+\lambda\tilde{b}_1C+\lambda\tilde{b}_2CK_1+\lambda b_2D(\theta K_1)+\lambda\tilde{b}_3CK_2+\lambda b_3D(\theta K_2)\\
&=I+\lambda\tilde{b}_1C+0+\frac{-b_2}{a_{22}}(I+\lambda\tilde{a}_{21}C)+0+\frac{-b_3}{a_{33}}(I+\lambda\tilde{a}_{31}C)+\frac{b_3a_{32}}{a_{22}a_{33}}(I+\lambda\tilde{a}_{21}C)\\
&=\left(1-\frac{b_2}{a_{22}}-\frac{b_3}{a_{33}}+\frac{a_{32}b_3}{a_{22}a_{33}}\right)I+\lambda\left(\tilde{b}_1-\frac{\tilde{a}_{21}b_2}{a_{22}}-\frac{\tilde{a}_{31}b_3}{a_{33}}+\frac{\tilde{a}_{21}a_{32}b_3}{a_{22}a_{33}}\right)C.
\end{aligned}$$

With this formulation of the limit of K and the continuity of $\rho(K)$ in θ, it can be shown that

$$\lim_{\theta\to\infty}\rho(K)=\max_{\kappa\in\mathrm{eig}(C(z))}\left|1-\frac{b_2}{a_{22}}-\frac{b_3}{a_{33}}+\frac{a_{32}b_3}{a_{22}a_{33}}+\lambda\alpha\kappa\right|.$$

This finishes the proof of Lemma 4.10 for $(2,3,p)$ IMEX methods with a P^1-DG spatial discretization.